Ferroelectricity in Barium Titanate Nanoshells

A Thesis

Submitted to the Faculty

of

Drexel University

by

Michael T. Coster

in partial fulfillment of the requirements for the degree

of

Master of Science

September 1, 2011

Dedicated to Eya.

Acknowledgements

I would first like to thank Dr. Spanier for the opportunity to work in his lab group for the last four and a half years. I was given the chance to learn things well beyond the scope of the classroom which have been invaluable as I move on to start my career after school. In my freshman year I joined the research group and it has been a rewarding experience and I owe all of that to Dr. Spanier.

He introduced me to Dr. Stephen Nonnenmann who served as my mentor for a few years before he graduated last year. His willingness to help me and patience when I first started are certainly more than I could personally portray. He taught me almost everything I know and I certainly wouldn't be here if it were not for him. He was a great friend and along with Rahul Joseph and Ron Martin made the lab a fun place in my first three years.

Throughout my time here there have been a number of guys who have remained constant, them being Terrence McGuckin, Oren Leaffer and Eric Gallo. For this project, Terrence is responsible for making the device testing interface while Oren developed most of the code implemented for the theoretical work and coercive voltage calculation. Eric has been especially fun to work with and I think that whenever I had a problem or a question, he was the first I would go to. For the most part he would be willing to listen and for that I thank him. Everyone needs someone like Eric and Steve to depend on when things don't quite add up!

For this project in particular, Stephanie Johnson has been a wonderful associate, having acted as my mentor and performing the PFM measurements. She's quickly become a PFM expert in her 3 or so years here and her experience is priceless. Though I don't think she has a future playing fantasy football, she's definitely destined to be

a great scientist! The same can be said of Guannan Chen who has also helped me along the way. His work-ethic and commitment to what he believes are great assets and anyone willing to argue facts with Eric is OK in my book!

I'd like to thank everyone else in the Spanier Group who has been here over the years. My fellow undergrads Brian Beatty, who performed the XRD work for this study, and Nick Bruzzese always provided some relief from lab work. Dr. Greg Soja, though his stay with us shorter, also provided some comic relief haha! Chris Hawley, Maria Torres and the rest of the group, present and past also deserve thanks for making my term with the Spanier Group a memorable one.

At this point in the acknowledgments my mother is probably reading thinking "Okay Mike when do you mention your family?" so I'll do that now! Without a doubt none of my accomplishments would have be possible without the support of my mom, Stephanie, dad, Harry and sister, Caitlynn. Though it has not been an easy ride, I think the places that I've gone and the things I've done have led me to a great place. I would have never gotten here if they hadn't been along the ride with me! I am also lucky enough to have a great extended family including many aunts and uncles who I think sincerely care how I did at school when they asked me during one the of family parties we have each year. I couldn't imagine it any other way.

Finally, college would not be complete without the many friends I have had and the brothers of Pi Kappa Phi that I've had the privilege to be associated with. While my studies might not have always been their first priority, they provided a good balance alongside schoolwork that kept me somewhat sane over the past few years.

With that I would like to conclude my acknowledgments by thanking Drexel for being the best 5 years I could have asked for.

Contents

List of Figures

Abstract

The ever decreasing dimensions of electronic devices introduce new difficulties in ensuring the stability and quality of their components. Ferroelectric materials have been limited in their application at the extreme nanoscale due to the increasing effects of depolarizing fields lending to instability in their polarization states. To combat these detrimental effects, curvature is introduced by way of a core-shell nanowire system employing a gold core and a ferroelectric barium titanate shell. Static piezoresponse force microscopy measurements reveal a renewed stability in ferroelectric polarization where the curvature of enough to reduce the effect of depolarizing fields. The stress induced by curvature also brings about a migration of the Curie temperature of barium titanate to above its bulk value, perhaps suggesting the material's increased viability as a stable ferroelectric on the nanoscale.

Chapter 1

Introduction

Ferroelectric (FE) materials find application in non-volatile memory devices due to their ability to hold a stable, polarized electric state. These states can be read in the conventional Boolean logic states, assigned a '0' or '1' based on the difference between their 'up' and 'down' states along the c-axis of the unit shell. The ability to control these states using an external electrical field has been extensively investigated in a number of different materials [1, 2]. Other factors such as external and internal stress fields can also have an effect on the polarization of these bulk materials [3]. It has been shown that as the dimensions of FE thin films decrease further into the nanoscale, these stresses can produce a depolarizing field effect [4]. To overcome this depolarizing field, a system which introduces stress due to extreme curvature in thin films is proposed.

In a previous study, the size dependence of polarization in $PbZr_xTi_{1-x}O_3$ (PZT) nanoshells was investigated in order to verify the ability to overcome depolarizing effects due to surface stresses [2, 5]. The stresses destabilize the orientation of the polarization thus creating an opposing layer that nullifies the polarization of the rest of the film. As memory device densities increase, it will require that devices become

smaller, thus increasing the effect that these stresses will have on device performance. In the study mentioned, the stress associated with extreme curvature effectively reduced the depolarizing field while enhancing the polarization of the thin film [5]. This enhancement will lead to more stable polarization states and ferroelectric devices as the dimensions continue to shrink.

Bulk lead-zirconium-titanate is ferroelectric up to 693 K, its Curie temperature (T_C), and exhibits a large polarizability compared to other FE materials room temperature. For these reasons, it would be considered a good candidate for use in FE random access memory (FeRAM) devices. However, the inclusion of lead is unfavorable due to its toxicity. In order for curved thin films to find a home in real devices, they must be synthesized with more environmentally-friendly materials. One of the pioneering materials to start the ferroelectric revolution, having been discovered during the Second World War, is barium titanate (BTO). This material has been tested for many years due to its simplicity and has found application in condensers and other electronic devices [6].

Barium titanate has an experimentally accessible Curie temperature of about 393 K, lending to its use in Curie temperature migration experiments [1]. The thermodynamic transition which occurs at T_C between the ferroelectric and paraelectric state is important for understanding the limits of FE devices. This transition is a second order transition so as temperature increases, the strength and magnitude of polarization will continuously decrease. With the introduction of extreme curvature to the film, it is expected that the polarization will be enhanced, prolonging this decrease and effectively increasing the material's Curie temperature. A core-shell (metal-ferroelectric) nanowire geometry is employed to introduce this curvature to the thin film.

Chapter 2 will introduce the kinetics behind the ferroelectric state and provide pertinent information about BTO in regards to this study. Given that the end goal

for the work is to verify the migration of the material's Curie temperature, there will be a summary of what this transition entails and how it is effected by size. Test devices are made via a templated growth sequence before lithography and subsequent evaporations are used to isolate individual nanowire devices. Their synthesis will be described in chapter 3. The procedure for testing the devices using piezoresponse force microscopy and other possible ways will be described in chapter 4. A discussion of the implications of the results as well as some theoretical work and concluding thoughts will be included in chapter 5. Chapter 6 includes some closing remarks.

1.1 Background

The basis of this project comes from the inability to easily test experimentally the phase transition at PZT's Curie temperature by measuring ferroelectric response in nanoshells. Theoretical work, outlined in chapter 6 proposes that curvature in nanoshells can change the PZT's Curie temperature, as represented in figure 1.1 (from [1]). Barium titanate has a lower Curie temperature so it is easier to perform measurements as it will only require temperatures of roughly 120°C. Similar theoretical progressions of BTO's Curie temperature are also presented having found the appropriate coefficients to perform the calculations.

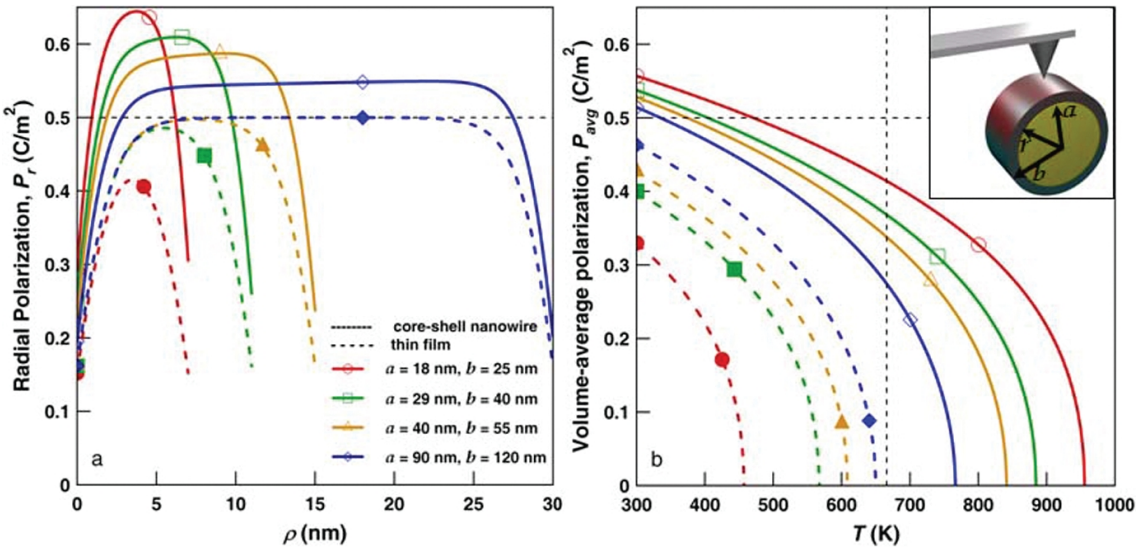

Figure 1.1: A modified Landau-Ginzburg equation can map polarization radially in a thin film and shell, as shown on the *left*. When averaged at different temperatures on the *right*, a change in Curie temperature as function of curvature and shell thickness is revealed. These graphs were completed for PZT in the previous study mentioned.

Chapter 2

Fundamentals of Ferroelectricity

2.1 General

Perovskites, which can be ferroelectric materials, occur in the ABO_3 formation where A and B represent metals. The three oxygen atoms are located in the center of the faces of an FCC structure while one metal atom is in the center of the unit cell and the other is located at the eight corners of a tetragonal structure. Figure 2.1 (from [7]) shows the perovskite structure when there is no strain applied.

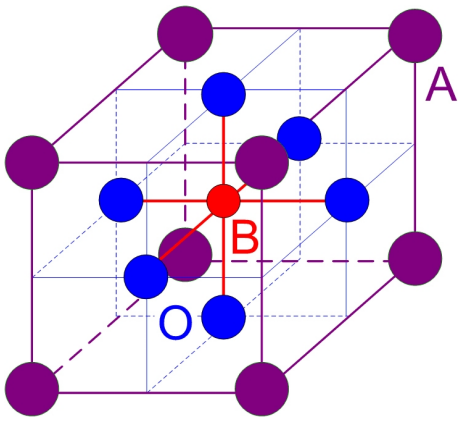

Figure 2.1: Perovskite structure for functional oxide ABO_3.

The order parameter, a property used to describe its phase symmetry associated with the arrangement of atoms, is the polarization of the material. Ferroelectric polarization results from a displacement of the center atom of the structure creating a dipole. In BTO, this displacement occurs along the c-direction. When all the dipoles of a material are aligned, it will maintain a non-zero electric field. The direction the center atom moves is dependent on the applied electric field around the material. Both directions are equal energetically, and the overall energy plot for polarization is shown in figure 2.2 (from [8]).

Figure 2.2 shows that in the ferroelectric state, a non-polar configuration, corresponding to the peak in the middle of the graph is unstable and not energetically favorable. This barrier can be overcome with energy provided by an external electric field. Doing so will cause the center ion to gradually move from one location to another, called switching, accounting for its characterization as a second order transition. As temperature increases, the peak will continuously decrease until the Curie temperature is reached. This is the temperature where the transition from a ferroelectric to paraelectric material occurs and is also second order. In the paraelectric state, it is no longer energetically favorable to create polarization states. The graph will simply be a parabola with the minimum at zero-displacement.

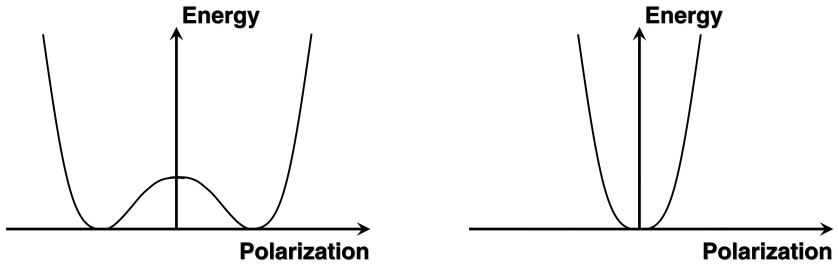

Figure 2.2: Energy and polarization profiles for a FE material below T_C (*left*) and above T_C (*right*).

2.2 Piezoelectricity

The piezoelectric (PE) effect defines the relationship between the electronic charge of a material and a strain field in a certain crystallographic direction. Under stress there will be a change in the material's geometry and a dipole will be created. What makes piezoelectricity even more dynamic is the ability for a strain to be induced by applying an external electric field to the same material. This is known as the converse piezoelectric effect [8].

For the sake of definition, piezoelectrics are materials that possess the ability to polarize electronically. Ferroelectrics are piezoelectric and their polarization can be manipulated via external electric fields in addition to external stresses.

2.3 Thermodynamics and Ferroelectricity

The favorable energetic polarization states can be described using Landau's theory for second order transitions. The simplified version of Landau's theory is given as equation 2.1.

$$G = G_0 + \alpha\eta + A\eta^2 + C\eta^3 + B\eta^4$$

Landau's equation for Gibbs free energy [9]. A, B, C and α are material dependent Laudau coefficients and η is representative of the order parameter. (2.1)

In the case of ferroelectricity, the α and C terms, along with the other odd coefficients, go to zero for symmetry purposes. The other coefficients are material dependent and get different constants based on their contributions. Also, the order parameter turns into polarization so that for ferroelectricity, the Gibbs free energy equation looks like that given in equation 2.2. Here, the coefficients B and C are both temperature dependent and involve relationships of bond strengths and stress. [10]

$$G = \frac{\alpha_0}{2}(T - T_C)P^2 + \frac{B}{4}P^4 + \frac{C}{6}P^6 + ...$$

Landau equation for ferroelectricity [10]. α_0. B and C are material Landau coefficients and the exponents change due to the transition's second-order characteristics. It is brought out to the sixth power for simplicity and contribution of the coefficient shown. (2.2)

2.4 Nanoscale Limitations

The basis of this project is to explore the effects that introducing curvature into FE thin films can have on the ferroelectric behavior of the material. Bulk polarizations can generally be achieved in films greater than 100 nm in thickness but as the thickness decreases it can decrease the ability for the material to fully polarize. This inability to produce stable FE states is brought upon by the surface effects including stresses introduced at the nanoscale. Depolarizing fields result in unstable unit cells at or near the surface whose dipole moments can oppose that of the material further from

the surface. This layer can effectively nullify the FE's overall electric state.

Surface charges associated with interfaces in FE devices can also produce a decrease in polarizability in thin films [11]. As the FE material undergoes its deformation, thus creating an inherent electric field, opposing charges will collect on the surface in an attempt to nullify them. When metals are involved as the electrodes, free electrons will screen these charges and create two same-sign dipoles at the interface. This will have detrimental effects on the materials ability to switch in ultra thin films on the order of 10 unit cells [11]. In typical thin films on the order of a few nanometers to 100 nm, these surface charges will have enough of an effect so to suppress the FE's polarization [8, 11].

Given the way that surface charges can disrupt a thin film's ability to polarize, multiple attempts have been made to overcome them. These include introducing other stress fields - the goal of this study - adding various chemical adsorbates and experimenting with different superlattices [12]. Past attempts at making strain variation have come in the form of lattice mismatches at the interface to create a deformation to the lattice constant [11]. Chemical environments can be changed by introducing different chemical species, such as oxygen to flood the surface of the materials. Chemi-absorbed molecules can result in a stretching in the bonds along the surface of the FE material and combat the effects of surface charges [13]. Various superlattices have been experimented with as well to control the deformation and ordering of polarization fields toward interfaces and throughout the films [6].

Along with the change in polarization stability, there is also a migration of the Curie temperature as the dimensions of the FE materials decrease [1]. At small thicknesses below 100 nm the FE will become unstable enough so that it can not perform like a ferroelectric at temperatures a bulk sample could withstand. This means that it will take less energy to transform the material from FE to paraelectric. In device

applications, less heat or energy would be required to lose a possible stored data state. It is the goal of adding curvature to reverse this decrease in stability and verify that there is an increase in the material's Curie temperature at small dimensions. This will make the material more stable and ideal for electronic applications. To test these characteristics, core-shell nanowire devices were fabricated, as outlined in chapter 3.

Chapter 3

Test Device Fabrication

3.1 Piezoresponse Force Microscopy Measurements

3.1.1 Bottom Up Synthesis

Many two-dimensional electronic devices are fabricated using a "top-down" method which involves the deposition of various layers of metals, oxides and other materials before a subsequent series of etching steps result in a device. As devices get smaller, the ability to make these devices is limited by current photolithography capabilities. Top-down processes are often difficult in cases where the devices are non-planar, as it would prove difficult to etch materials in such a fashion. Thus, a "bottom-up" synthesis process was developed that allows controlled growth of non-planar devices in both templated and template-free settings. Nanowire growth is performed in both manners, but for this study the growth of the Au-$BaTiO_3$ wires was completed using anodic aluminum oxide (AAO) templates.

3.1.2 Anodic Aluminum Oxide Templates

To aid in the fabrication of the core-shell nanowire structure, anodic aluminum oxide templates are used. Through various growth conditions achieved by changing growth temperature and potential, the diameter of cylindrical pores within the templates can be controlled allowing for the growth of different size nanowires. These kinds of templates are often used in nanotube growth processes which require sol-gels because of the ability for the sol-gel to wet the pore walls [14]. Ferroelectric perovskite sol-gels including lead titanate, lead zirconium titanate and strontium bismuth titanate have all been shown to produce nanotubes after wetting pore walls.

Some templates for this project were purchased commercially from Whatman Inc. (Anapore ∼100 nm and ∼200 nm) while others requiring smaller power sizes are grown in the lab. Laboratory-grown templates were fabricated via a two-step anodization process from high-purity Aluminum sheets (Alfa Aesar Puratronic 99.9995% #43777). Process conditions for growth in .3 molar oxalic acid are 1°C and 30 - 50 V for different pore sizes. These conditions and the commercial templates allow for devices of diameters ∼50 nm to ∼250 nm. The procedure for growth is as follows:

1. Sonicate the Al sheet in acetone for 10 min to clean

2. Electropolish the aluminum for 5 minutes in a 1:1 mixture of perchloric acid and ethanol at for 3 minutes

3. The anodization of the Al sheet occurs in a custom electrochemical cell designed to expose a selected area to the oxalic acid. The first step lasts roughly an hour.

4. The first layer must be removed and it is done so with a mixture of chromic and phosphoric acids at 60°C for an hour. This leaves the textured surface of the Al behind.

5. The second step is run at the same conditions but at an upwards of 60 hrs, a longer run producing a thicker oxide.

6. To isolate the oxide template, the Al sheet is removed using $HgCl_2$ and rinsed in water.

7. To open the pores a .05 wt.% phosphoric acid solution is used. The time varies for the pore size desired.

3.1.3 Sol-Gel Processing

Sol-gels are polymeric suspensions of colloids between 1 and 100 nm in diameter. Ferroelectric oxide sol-gels, like $BaTiO_3$, are made through a hydrolysis and polycondensation process using metallic alkoxides. The sol-gel used in this study, as well as many others involving $BaTiO_3$, is commercially available from Chemat Inc. To achieve a perovskite phase from the polymer once it is inside the template, an annealing step is performed at 700°C for 2 hours increasing to the target temperature at 10°C/min. To verify the tetragonal phase of BTO, room temperature x-ray diffraction was used and the results are included in Figure 3.1.

Isolated nanotubes of 200 nm in diameter and without a core were used for the measurement after being dispersed on a Si substrate. The major highlight in determining that the diffraction pattern represents that of a tetragonal structure is the splitting of a 100 and an 001 peak. To have a better view of the peaks for the BTO, a peak fitting program within MATLAB was used and comprises the bottom graph of Figure 3.1. The 100 and 001 peaks represent the a and c lattice parameters respectively, corresponding to lengths of 3.87 and 4.03 Å. This difference is roughly 4 percent, greater than the difference shown in previous measurements on BTO powders [15]. The XRD performed on powders revealed a 1 percent difference where the a

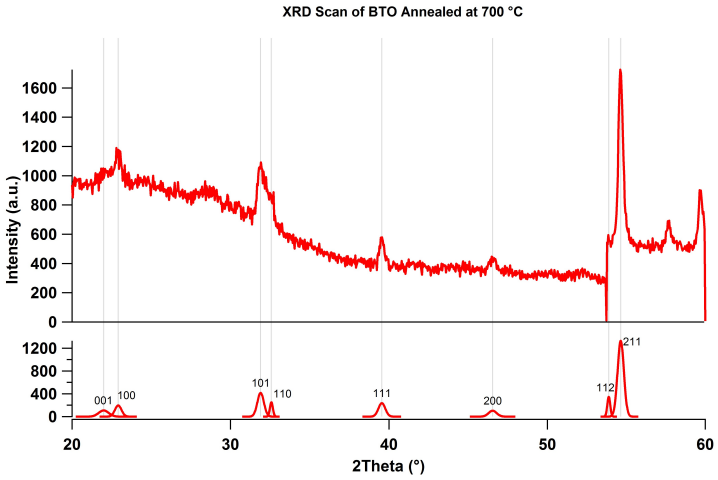

Figure 3.1: XRD scan of tetragonal 200 nm BTO nanotubes dispersed on Si substrate.

lattice parameter was 3.99 Å [15]. It is possible that the difference in the relationship between the 100 and 001 peaks are influenced by the curvature of the nanotube.

3.1.4 Electrodeposition of Gold Cores

Another advantage of using AAO templates is their employment in cathodic reduction of metals to grow one-dimensional nanostructures. Successful deposition of gold, copper, colbalt and silver have been reported [16]. To prepare the templates for electrochemistry, there is first an application of a conductive back-coat on the template. This comes in the form of a 150 to 200 nm thick layer of silver deposited via thermal evaporation. An electrochemical cell is completed using the template - after it is attached to a wire and is back-coated with a protective, non-conductive layer - and a platinum counter electrode.

Sulfite metal salts are used in this reduction reaction due to their nontoxicity and compatibility with electron beam processes [8]. To grow the gold cores, silver (Technic Silver Cyless) is first electrodeposited at a constant current density of roughly 1.25 A/cm^2 to ensure that there is silver capping the end of each pore. This allows for

the gold deposition, which is performed next, to only grow inside the pores. This is performed at a slightly reduced current density between .3 and 1 A/Cm^2 in a gold (Technic Gold 25) solution. Figure 3.2 shows the gold wires within the template after the Ag has been dissolved away using nitric acid. A top view of a custom grown template with pores on the order of 40 nm is also shown in Figure 3.2.

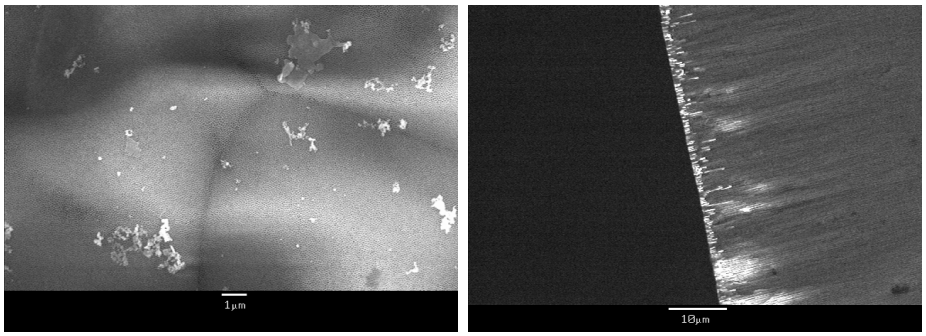

Figure 3.2: *Left* SEM top view images of AAO template; *Right* SEM back-scatter image of AAO template cross-section showing brighter segments of Au cores.

3.1.5 Electron Beam Lithography and Metal Evaporation

In order to complete the test structures they must be contacted in a way that allows electronic probing to the nanowire core. This task is performed using electron-beam lithography in an SEM using the Nanometer Pattern Generation System (NPGS). This system uses alignment markers to focus in on a selected area to write patterns in a three layer PMMA (950 K, 100 K, 950 K) electron beam resist. The patterns expose areas to connect the nanowires to pre-fabricated bond pads as shown in a DesignCAD file in Figure 3.3.

After patterns are written, the resist must be developed in a 3:1 mixture of 2-propanol:4-methyl-2-pentanone (MIBK) for ∼70 seconds. With the wire exposed through the patterns, a buffered oxide etch (BOE) is used to remove the FE shell and

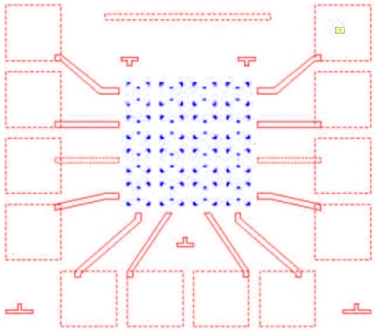

Figure 3.3: DesignCAD file of Alignment Markers and Bond Pads.

expose the metal core. A short exposure to an oxygen plasma cleaner ensures there is no residue that will disrupt a clean contact. Finally, the samples are placed in the thermal evaporator to deposit a 10-200 nm layer of chrome-gold. The chrome acts as an adhesion layer on both the silicon wafer and the nanowire. Without this layer, the chances of delamination occurring is greatly increased.

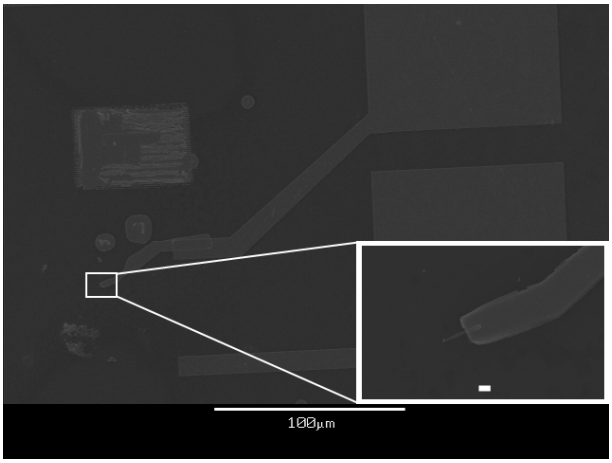

Figure 3.4: Image of a contacted wire with the bond pads. The scale bar in the inset is 1 μm.

To finalize the contacting of the wire, an example of which is shown in Figure 3.4, the remaining photoresist that was not exposed during lithography is removed via a liftoff in acetone. The three layer photoresist is responsible for ensuring that the

liftoff is clean and the edges are sharp. The chip is then wirebonded into a chip-carrier specially designed with an interface to allow for electronic probing within the Atomic Force Microscope. The special design allows for each wire to be tested individually by electrically biasing the metal core through a series of wire-bonds and making the actual wire accessible to an AFM tip. The final test device is shown in Figure 3.5.

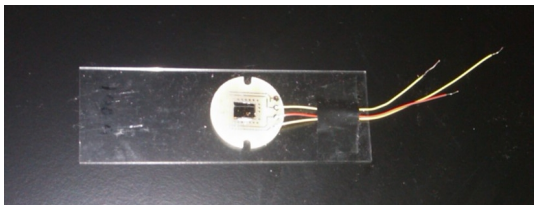

Figure 3.5: A finalized test device consists of the sample, glass-slide, a chip carrier and wire bonds for electronic probing.

3.2 Dielectric Constant Measurement Devices

The fabrication for the devices which were measured for their capacitance was very similar to the steps outlined in the previous section. Wire cores were contacted using electron beam lithography using the same etching and evaporation techniques. Instead of leaving the other end free to be probed with an AFM, the other side was then contacted via a second electron beam lithography step but the shell was not etched. The sample geometry can be likened to a capacitor where the inner and outer walls of the shell act as the interfaces and the inner gold core and the wrapped gold contact act as the plates. An example of a completed devices is shown in Figure 3.6.

These devices were made on both silicon and sapphire substrates. The sapphire substrates required a little more work due to their very high insulating qualities. Their surfaces charge-up very quickly when exposed to an electron beam, thus making it impossible to perform e-beam lithography directly on them. Thus, a conductive layer

of silver is evaporated onto the sample on top the electron beam resist. The silver is transparent to the backscatter detector in the SEM and provides a route away from the sample for the incident electrons, thus greatly reducing surface charging.

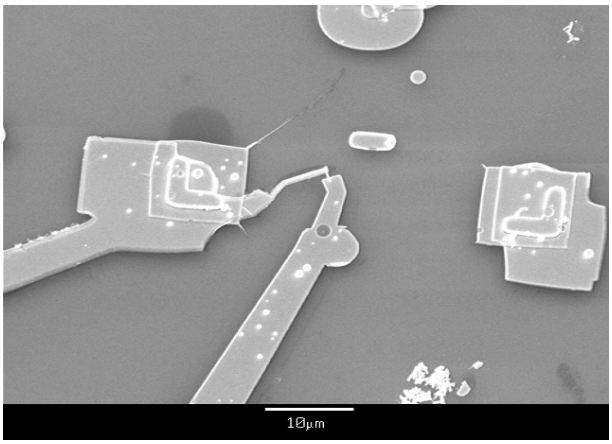

Figure 3.6: Completed 200 nm BTO core-shell nanowire device for capacitance measurements.

Chapter 4

Ferroelectricity in a Nanoshell

The atomic probe test procedure for these nanoshell devices has been used often for probing nanoscale systems [1, 2, 5, 17]. Whether it is for nanowires or other nanostructures, it is possible to probe individual structures with an atomic force microscope due in part to its high resolution. This form of microscopy, often referred to as AFM, works using the principle of measuring the interaction of a cantilever tip and a sample, in this case, an individual nanowire. The interactions include van der waals forces as well as charge or chemical interactions if the tip is functionalized appropriately [17].

Ultimately, the interaction between the tip and the sample is governed by Hooke's law for springs. As the tip approaches the surface, it will become attracted to the surface and bend towards it. The amount of bending will depend on the strength of the attraction and the elasticity of the cantilever. As the tip's height decreases and it continues to get closer to the sample, the interaction will become repulsive and the tip will bend upwards. These acts of bending reflect the AFM's laser back onto the photodiode, relaying where the tip is in relation to the surface. The magnitude of the bending is what gives rise to topology information for the sample. Figure 4.1

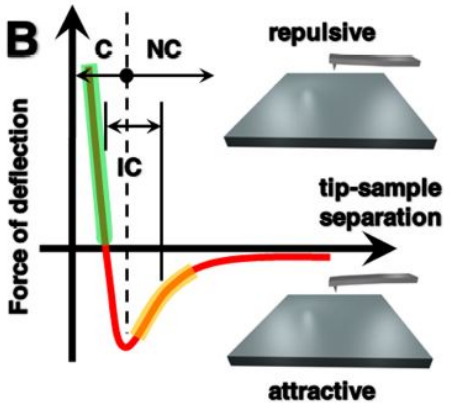

Figure 4.1: Schematic for the tip-sample interactions. C, IC, and NC stand for Contact, Intermittent-contact and Non-Contact modes, respectively.

(from [8]) displays the attractive and repulsive regimes of the tip-sample interaction.

4.1 Piezoresponse Force Microscopy

Scanning probe microscopy is a technique which allows for the measurement of a selected area to understand the topography or other properties of a surface or structure. In the attempt to measure piezoelectricity, piezoresponse force microscopy (PFM) is used. PFM is classified by the application of an AC voltage to the cantilever tip to induce a converse piezoelectric response [8] within the sample. When the voltage can induce a strain change in the FE, there will be a height change and the cantilever will deflect along with it. The use of a lock-in amplifier can split the signal to reveal information about the magnitude and orientation of the strain state and the ferroelectric polarization of the material [8].

Along with the scanning variation of PFM there is also a static hysteresis mode. In this setup, the tip is brought in contact with the sample, i.e. the nanowire, and is held there. A triangle wave is applied to the core electrode and the tip is deflected due to gradual increase and decrease in polarization in the film. Once the wave is

complete, the resulting graph reveals a piezoelectric hysteresis curve representative of the peizoelectric d_{33} coefficient, which is the direction associated with the film's thickness. Static hysteresis mode has been demonstrated in hollow FE nanotubes but scanning modes are not possible due to the likelihood for the tubes to break [18]. In this experiment, the static mode of measuring ferroelectric piezoelectric hysteresis is implemented.

4.2 Dielectric Constant Measurements

When the BTO undergoes a phase transition, there will be a noticeable change in its dielectric properties. The dielectric constant will change in a consistent manner with temperature until a phase transition occurs. This change has been demonstrated in BTO grains as small as 8 nm in size [19]. There is a steady increase in the dielectric constant as the temperature is raised up to the sample's Curie temperature. Then there will be a discernible peak and it will start to decrease as the temperature continues to climb.

Preliminary IV tests of these devices were performed with the goal of determining the threshold voltage for these samples. Using an electronic probestation under vacuum, a voltage was applied across the shell thickness by a power source and the current was measured. Though they did not yield a threshold voltage before exploding, these IVs, such as the one shown in Figure 4.2, served to display that the films were robust enough to provide a screen between the two electrodes. This was the first evidence that there was indeed a shell surrounding the core. The IV curve shape is indicative of a Schottky contact, which could be expected with an oxide across the interface between contacts.

The graph itself, a result of an IV test on a 200 nm sample, reveals that there

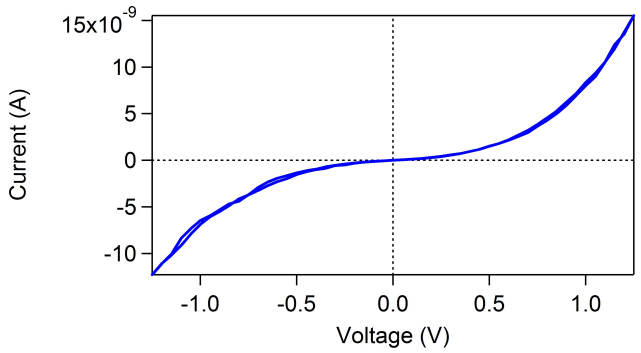

Figure 4.2: Current-Voltage measurement across BTO 200 nm nanoshell.

is a little by way of capacitance. The curve appears to lend itself to a fair amount of leakage across the shell. It could also be due to the SiO_2 substrate, which in its own right, will have a capacitance on the order of the single nanowire device. This is why a method using sapphire substrates is proposed for measuring capacitance, as its capacitance is considerably lower. The perform the measurements a potential is applied across the shell in a DC sweep mode while an LCR meter measures the capacitance. Using the equation $C = \epsilon_d \frac{A}{d}$ where d is the shell thickness, the dielectric constant can be determined when capacitance and current are measured. Changing the temperature intermediately to above the Curie temperature and completing subsequent measurements will exposed a trend in the change of the dielectric properties of the material with temperature.

Chapter 5

Curvature-Mediated Ferroelectric Properties

The benefit of the fabrication process outlined in Ch. 3 is that curvature is introduced into thin films. The progression from a bulk material to a thin film means that the stresses associated with the interfaces are more enhanced and will have a greater effect the FE state of the material. To overcome the depolarizing effects of these surfaces, curvature is introduced to add stresses within the plane of the thin film. In the previous study on PZT, the curvature was found to not only restore but to even enhance the polarization of the material [5]. It has been shown theoretically that there is a similar expectation in BTO by applying a variation of the Landau-Ginzburg equation [5, 20].

Appendix A introduces code written in MATLAB^{TM}for determining the radial polarization of a FE nanoshell and its Curie temperature. This code was developed as part of the previous study mentioned and was modified to consider the material properties of BTO [5, 8]. The Landau-Ginzburg equation for the Gibbs free energy in the system is given in equation 5.1. The Landau coefficients A, B and C are provided

from previous experiments and are shown in appendix B along with electrostrictive coefficients [21, 22]. The g term considers the surface energies and can vary the $\mathrm{P}_r(\mathrm{r})$ term, which is the radial polarization term. It depends on the radial position in the shell. The depolarizing field is represented by this term combined with $\mathrm{E}_d(\mathrm{r})$. The depolarizing field is averaged across the shell thickness an yields a simplified form of $\mathrm{E}_d(\mathrm{r}) = 4\pi\left[P_r(r) - \overline{P}_r\right]$ [23].

$$G = \int_a^b \left[\frac{A}{2}P_r\left(r\right)^2 + \frac{B}{4}P_r\left(r\right)^4 + \frac{C}{6}P_r\left(r\right)^6 + \frac{1}{2}g\left(\nabla P_r\right)^2 - E_d\left(r\right)P_r\left(r\right)\right]rdr + \frac{D}{2\delta}\int_S P_r^2 dS$$

Gibbs free energy equation. (5.1)

The progression of radial polarization across the FE shell thickness is a result of an integration of the Euler-Lagrange equation, given as equation 5.2. The integration was performed using a nonlinear finite-difference method considering electrostatic boundaries. The $\hat{A}$ is equal to $A - 2Q_{11}\sigma_{rr}(r) - 2Q_{12}\sigma_{\varphi\varphi}(r)$ where the $\sigma_{rr}(r)$ and $\sigma_{\varphi\varphi}(r)$ are defined in equation 5.3. They are the radial and azimuthal stresses, respectively [20].

$$g\nabla^2 P_r\left(r\right) = \hat{A}P_r\left(r\right) + BP_r^3\left(r\right) + CP_r^5\left(r\right) - E_d\left(r\right)$$

Euler-Lagrange equation. (5.2)

$$\sigma_{rr,\varphi\varphi}(r) = \frac{a^2}{b^2 - a^2}\left(1 \mp \frac{b^2}{r^2}\right) P_{a\rho} - \frac{a^2}{b^2 - a^2}\left(1 \mp \frac{a^2}{r^2}\right) P_{b\rho}$$

Radial and azimuthal stress equations; a and b are the inside and outside surfaces of the nanoshell which the ρ term is the radial position [8]. (5.3)

The stresses from equation 5.3 constitute the Lamé problem based on the surface tension, μ, of BTO which is assumed to be 5 N/m [20]. This term also drives the thickness of the shells when they form on the pores during fabrication. It is the same value for PZT, thus making it valid to select similar shell thicknesses and radii for theoretical measurements in BTO.

The result of the theoretical calculations are shown in Figures 5.1 and 5.2. In Figure 5.1, the average polarization in the shell is shown as a function of temperature. As the temperature approaches the bulk Curie temp of 393 K, there are migrations associated with the thickness and stress contributions. The dotted lines accurately portray the instability of polarization in thin films as they continue to decrease in thickness. The Curie temperature of the thin films also decreases with thickness. The opposite is the case when curvature is introduced. There is an enhancement of both polarization and Curie temperature. At room temperature the polarization is higher than that found in typical bulk BTO samples when more stress related to curvature is introduced. The same goes for the Curie temperature, which is highest in the smaller shell where the curvature has a greater effect.

Figure 5.2 is the result of solving for the radial polarization. As evidenced by the decrease in polarization at both the inside and outside, there is the consideration of

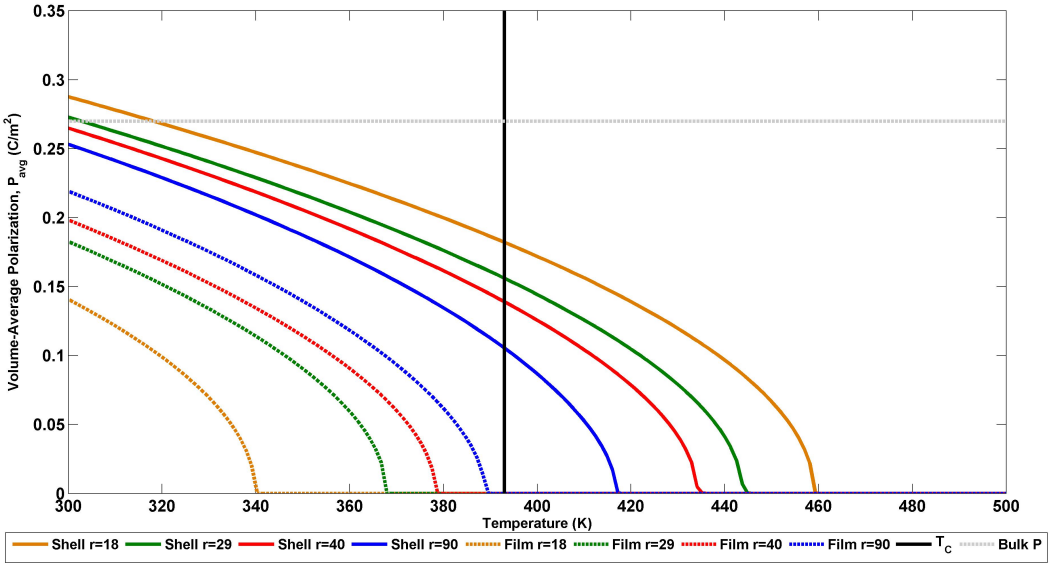

Figure 5.1: Volume-averaged radial polarization plotted as a function of T to show the eventual loss of polarization at the sample's Curie temperature.

surface stresses and the presence of a dead layer. As the shells decrease in thickness, the peak polarization is also effected by these surface contributions. Thin films will eventually lose all FE stability as they continue to decrease. In nanoshells with curvature induced stresses, there is an enhancement in the polarization which increases as the curvature does. The new stress fields introduced by curvature work to overcome those inherent to the thin films.

Both of these theoretical calculations are limited somewhat by their dependence on both the shell thickness and the shell's inner and outer surface radii. It is ultimately these values of inner and outer radius that determines how the results will look. For this study, sizes were chosen based on the size of the devices measured in the PZT study [2,5]. To summarize, the sample are referred to by their inner radius, i.e. 'Shell r=18' and 'Shell r = 40' are samples where the core's radius equals 18 and 40 nm, respectively. This inherently means that the inner surface of the nanoshell has a

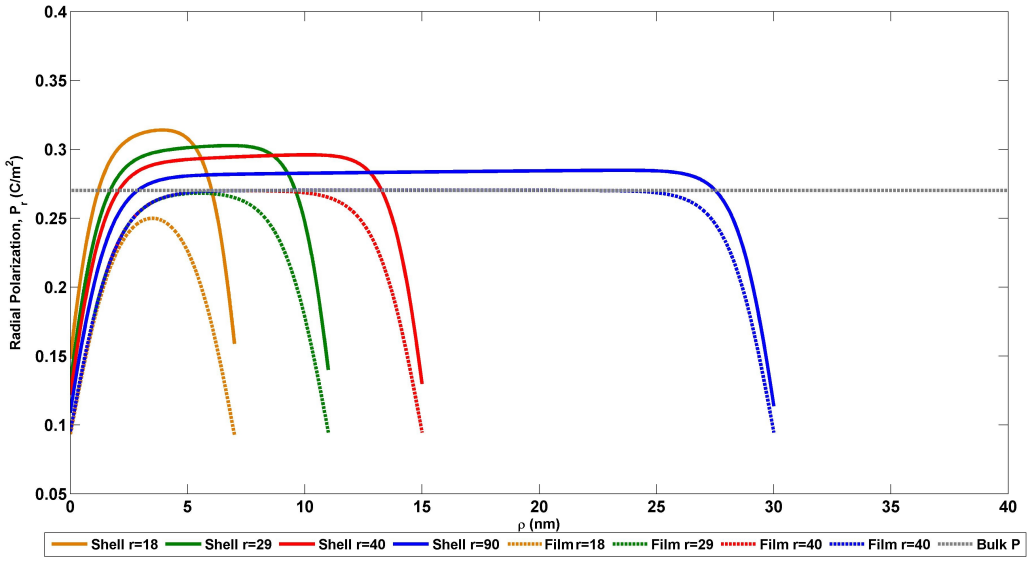

Figure 5.2: Radial polarization of a nanoshell starting at its inner surface and ending at its outer surface. ρ is a variable representative of the radial position within the nanoshell.

radius of the sample value. In Figure 5.2, the inner radius is at 0 nm in each sample and the thickness extends outward from that point. The thicknesses were also a result of the measurements performed with the PZT samples [2, 5]. Ultimately, both the curvature, dictated by the inner and outer radii, and the shell thickness, the difference between the two, will effect the results. Thus, their individual contributions can not be be accurately determined. It should not take away from the fact that they do indeed prove worthy of changing the polarizability of a FE material.

Bulk $BaTiO_3$ exhibits a spontaneous polarization of roughly 26 $\mu C/cm^2$, as determined experimentally [24]. The bulk numbers approached using this study are closer to 27 $\mu C/cm^2$, which is consistent with other calculated values [25]. Nevertheless, they match up quite well and the enhancement exhibited with the curved thin films is still valid theoretically.

5.1 Results

The goal of this study is to verify the theoretical migration of the Curie temperature in ferroelectric thin films, brought about by an extreme curvature achieved by use of a core-shell nanowire geometry. As stated previously, depolarizing fields within thin films can overcome the polarizing field, leaving the film's ability to hold a state more unstable as the dimensions of the thin film decrease. This instability is also present in the decrease of the ferroelectric material's Curie temperature as thickness decreases. Bulk films of BTO, generally regarded as 100 nm or greater, go through a phase transformation from ferroelectric to paraelectric between 383 and 393 K.

Results of PFM tests on two sizes of nanowires on the order of ∼100 nm and ∼200 nm in diameters are included, with each sample expected to have ferroelectric shells on the order of 20 nm and 30 nm, respectively. These thickness assumptions are based on the previous study using a similar sol gel process for the fabrication of the nanoshells [2, 8]. The viscosity of the sol gels were very similar and wet the pores is the same way so the shell thicknesses should be every similar. The thicknesses will eventually be verified using a transmission electron microscope to see the shell around the core. Nanowires on the order of 40 nm in diameter have also been grown but as of yet, have not been tested. It is expected that they will provide shells that are sub 10 nm in thickness, thus allowing for probing of even smaller shells, furthering the conclusions of this part of the study.

The PFM measurements were performed under ambient conditions in the dark. A sweeping voltage of ±10 V was applied slowly at 0.5 or 0.7 Hz to the core, providing the potential to the shell. The tip was placed on top of the wire after it had been mapped during a previous scanning mode topography measurement. The tip had an AC bias of 3 V applied to it as well to keep it in contact with the nanoshell. During

the measurement, the tip was in deflection feedback mode which reports on the tip's movement in the z-direction, i.e. radially on the nanowire.

Having performed PFM on the 100 and 200 nm wires, it is concluded that curvature can indeed enhance the of stability of polar states of BTO thin films. The deflection of the PFM tip was measured and converted into piezoresponse by considering the cantilever stiffness and lock-in sensitivity. Hysteretic behavior of the 100 and 200 nm wires were measured in a series of loops at different temperatures. As the temperature increases, the strength of the polarization will decrease, represented by a reduction in the loop areas.

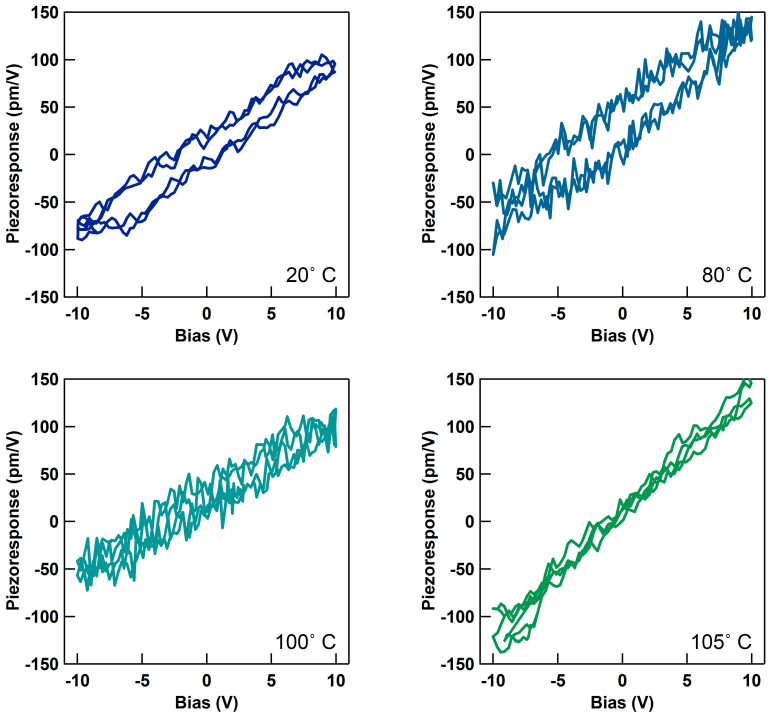

Figure 5.3: Piezoresponse loops for 200 nm diameter samples at various temperatures showing ferroelectric hysteresis decreasing to zero before the bulk Curie temperature.

The 200 nm nanowire's results are shown in Figure 5.3. Ferroelectric polarizations are shown at room temperature, roughly 20°C, at 80°C and at 100°C. The loops are

stable at each temperature and decrease and the temperature increases. There is no longer hysteresis present in the wires at 105°C, which is not in agreement with the proposed theoretical model. According to the model discussed earlier in this chapter, there should be a stable polarization at temperatures greater than 120°C, which would show the upward migration of the Curie temperature. However, in the case of these devices, the Curie temperature has decreased, a characteristic of thin films on the same order of thickness. There are a number of reasons why the effects of curvature did not reflect the theoretical results.

The theoretical calculations are simplified models and might not accurately consider what is happening in this real-life scenario. In sol-gel bottom-up fabrication, there can be a opportunity for films to exhibit defects or cracks as a result of poor film quality. These defects are thought to provide a stress relaxation to the film and could result in less enhancement by the film's curvature induced stress. It is also believed that these defects could also result in the offset shown in the graphs up the y-axis [8]. The IV curve presented in Figure 4.2 exhibits leakage characteristics, which could be blamed on the presence of defects in the shell.

In addition to the possibility of defects, there is a prospect that at this dimension, in ∼200 nm diameter wires with expected shell thickness of 30 nm, the curvature might simply not be enough, though the corresponding theoretical nanoshell, with r = 90 nm, suggests it would Theoretical data such as this has not been verified experimentally and this might point to the chance that it is incorrect. At the level of curvature, the shells could act as planar thin films in a local proximity, enough so that the curvature does not effect the depolarizing field. However, it is not to say that curvature cannot enhance polar stability because of the results obtained in the 100 nm wires that support the theory.

Figure 5.4 shows the results of a temperature study using PFM on the 100 nm

$BaTiO_3$ nanowires. There are stable polarization states measured up to 140°C, twenty degrees higher than the previously mentioned bulk Curie temperature of BTO. Given that the wires were fabricated in the same manner as the 200 nm wires, all variants including defects are in play and the only difference would be the curvature and shell thickness. The shell thickness in the 100 nm devices are most likely thinner than those in the 200 nm wires, given results of the previous study in BTO. A decrease in the thickness would lead to an even more unstable polarization if it not be for the introduction of the curvature. Conclusions can be drawn that at this scale, roughly half that of the 200 nm devices, the curvature is extreme enough to provide a stress field to combat the depolarizing field. At this scale, the Curie temperature is increased and the ferroelectricity of the thin films is enhanced.

Bulk barium titanate exhibits a piezoresponse d_{33} coefficient value of 100 pm/V [26]. At smaller dimensions below 100 nm, other measurements have shown a sharp decrease in this value for unstrained samples. At a thickness of 40 nm, the measured d_{33} coefficient value goes as low as 2 pm/V [27]. The BTO nanoshells here exceed this number greatly, staying close to 100 pm/V. This confirms the onset of a ferroelectric enhancement in the shells under the effects of the curvature.

Finally, by calculating the center of the loops and the intersections on the loops from that center point, the coercive voltages can be determined. This voltage can tell how much energy is required to switch a ferroelectric from one state to another. When a film is more stable, it will require more energy to switch so it would be expected that as the temperature increases, the coercive voltage will decrease. This progression is also visible in the decrease in the size of the piezoresponse loops.

The results of this calculation, for which the procedure code can be found as part of Appendix A, are shown in Figure 5.5. In the 100 nm samples, there is not an obvious transition, likely because measurements were not performed at temperatures

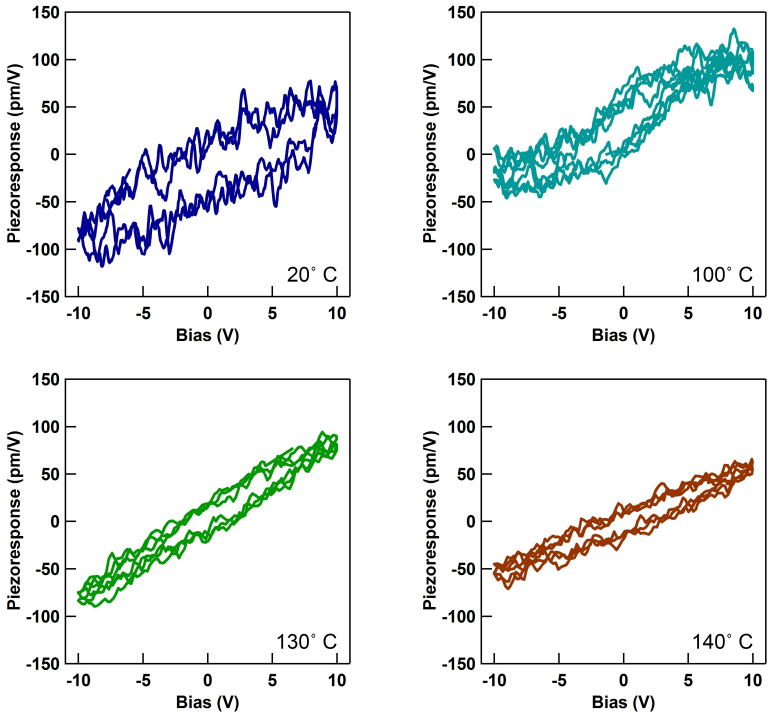

Figure 5.4: Piezoresponse loops for 100 nm diameter samples at various temperatures showing stable ferroelectric hysteresis at temperatures above the bulk T_C.

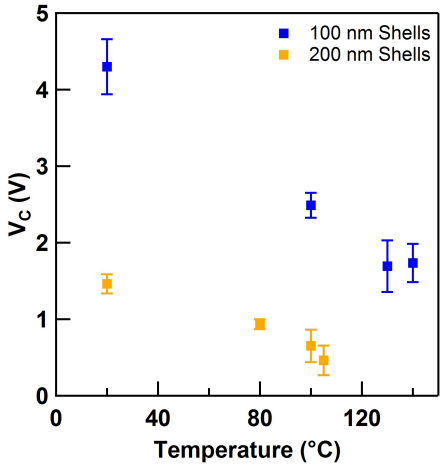

Figure 5.5: Coercive voltage graph for 100 nm and 200 nm samples at measured temperatures. Error bars added by determining the average V_C for each set of loops at each temperature and applying the standard deviation.

high enough to reach the new Curie temperature. The shape of the curve is also more linear than would be expected, especially compared to the results of the 200 nm samples. The shape of that curve clearly reveals the onset of a transition in the same region where the loop was closed in the previous round of measurements. This abrupt decay is reminiscent of the Landau-Ginsburg theoretical plots, and is related because the equations describe polarization dependence on applied fields. In a similar way, the coercive voltage will change with temperature in a manner similar to that of a second-order transition. The amplitude of the voltage is also quite smaller than the 100 nm sample overall, perhaps alluding to the instability cited by the degree of curvature possibly not having as great an effect as expected theoretically.

Chapter 6

Concluding Remarks

The conclusion of this Master's thesis work results in the confirmation that ferroelectric stability can be achieved at a temperature above a material's Curie temperature with the introduction of curvature and stresses associated with it. The bottom-up method of preparation, which I completed in full, having previously been used with a PZT shell, was adopted for use with barium titanate. The successful measurement of these devices suggests that this mode of fabrication and testing is valid for use in collecting data on ferroelectric materials at the nanoscale. Future work will certainly look to expand on the process with smaller wires which I have prepared and furthering the understanding of its results.

The study for BTO will continue with the measurement of 40 nm diameter nanowires where the films are predicted to be under 10 nm in thickness. The wires have been grown in lab-grown AAO templates in preparation for testing. A third size will give a more complete data set to accompany this study. The prospect of also testing the dielectric behavior may be pursued in the future as well. The phase transition will be viewable in a discontinuity of the dielectric constant across several temperatures. This will only serve to support the findings of PFM measurements.

While not totally necessary for this study, the inclusion TEM imaging for accurate measurements of shell thickness will be appropriate for a complete understanding of the devices. There are a number of other variables, such as comparing the results directly to planar thin films fabricated from the same sol gel using methods, that will increase the comprehensiveness of the study.

Bibliography

[1] Jonathan E. Spanier, Alexie M. Kolpak, Jeffrey J. Urban, Ilya Grinberg, Lian Ouyang, Wan Soo Yun, Andrew M. Rappe, and Hongkun Park. Ferroelectric phase transition in individual single-crystalline batio3 nanowires. *Nano Letters*, 6(4):735–739, 2006.

[2] Stephen S. Nonnenmann, Eric M. Gallo, Michael T. Coster, Gregory R. Soja, Craig L. Johnson, Rahul S. Joseph, and Jonathan E. Spanier. Piezoresponse through a ferroelectric nanotube wall. *Applied Physics Letters*, 95(23):232903, 2009.

[3] Z. H. Zhou, X. S. Gao, John Wang, K. Fujihara, S. Ramakrishna, and V. Nagarajan. Giant strain in $\mathrm{pbzr_{.2}ti_{.8}o_3}$ nanowires. *Applied Physics Letters*, 90(5):052902, 2007.

[4] V. Nagarajan, C. L. Jia, H. Kohlstedt, R. Waser, I. B. Misirlioglu, S. P. Alpay, and R. Ramesh. Misfit dislocations in nanoscale ferroelectric heterostructures. 86(19):192910, 2005.

[5] Stephen S. Nonnenmann, Oren D. Leaffer, Eric M. Gallo, Michael T. Coster, and Jonathan E. Spanier. Finite curvature-mediated ferroelectricity. *Nano Letters*, 10(2):542–546, 2010. PMID: 20067286.

[6] J. F. Scott. Applications of modern ferroelectrics. *Science*, 315(5814):954–959, 2007.

[7] Cheng-Shong Hong, Sheng-Yuan Chu, Wen-Chang Su, Ren-Chuan Chang, Hsiau-Hsian Nien, and Yung-Der Juang. Effects of the mno additives on the properties of pb($fe_{2/3}w_{1/3}$)–$pbtio_3$ relaxors: Comparison of empirical law and experimental results. *Journal of Applied Physics*, 101(5):054117, 2007.

[8] Stephen S. Nonnenmann. *Integrated non-planar ferroelectric nanostructures*. PhD thesis, Drexel University, 2010.

[9] Jeroen ven den Brink. Theory of condensed matter 2006. Course Website, 2006.

[10] Dan Ricinschi, Vasile Tura, Liliana Mitoseriu, and Masanori Okuyama. Landau theory-based analysis of grain-size dependence of ferroelectric-to-paraelectric phase transition and its thermal hysteresis in barium titanate ceramics. *Journal of Physics: Condensed Matter*, 11(6):1601, 1999.

[11] Javier Junquera and Philippe Ghosez. Critical thickness for ferroelectricity in perovskite ultrathin films. *Nature*, 422(6931):506–509, 2003.

[12] Stephen Nonnenmann and Jonathan Spanier. Ferroelectricity in chemical nanostructures: proximal probe characterization and the surface chemical environment. *Journal of Materials Science*, 44:5205–5213, 2009. 10.1007/s10853-009-3680-8.

[13] Stephen S. Nonnenmann, Eric M. Gallo, and Jonathan E. Spanier. Redox-based resistive switching in ferroelectric perovskite nanotubes. 97(10):102904, 2010.

[14] Yun Luo, Izabela Szafraniak, Nikolai D. Zakharov, Valanoor Nagarajan, Martin Steinhart, Ralf B. Wehrspohn, Joachim H. Wendorff, Ramamoorthy Ramesh,

and Marin Alexe. Nanoshell tubes of ferroelectric lead zirconate titanate and barium titanate. *Applied Physics Letters*, 83(3):440–442, 2003.

[15] Anthony R. West. *Solid State Chemistry and its Applications*. John Wiley Sons Ltd., June 1987.

[16] Mordechay Schlesinger. *Modern Electroplating, 4th Edition*. Wiley - Interscience, Aug. 10, 2010.

[17] S. Tiedke, T. Schmitz, K. Prume, A. Roelofs, T. Schneller, U. Kall, R. Waser, C. S. Ganpule, V. Nagarajan, A. Stanishevsky, and R. Ramesh. Direct hysteresis measurements of single nanosized ferroelectric capacitors contacted with an atomic force microscope. *Applied Physics Letters*, 79(22):3678–3680, 2001.

[18] Jongok Kim, Sun A Yang, Yong Chan Choi, Jin Kyu Han, Keum Ok Jeong, Yong Ju Yun, Dong Jik Kim, Sang Mo Yang, Doohee Yoon, Hyeonsik Cheong, Ki-Seog Chang, Tae Won Noh, and Sang Don Bu. Ferroelectricity in highly ordered arrays of ultra-thin-walled pb(zr,ti)o3 nanotubes composed of nanometer-sized perovskite crystallites. *Nano Letters*, 8(7):1813–1818, 2008. PMID: 18540654.

[19] Xiaohui Wang, Xiangyun Deng, Hai Wen, and Longtu Li. Phase transition and high dielectric constant of bulk dense nanograin barium titanate ceramics. *Applied Physics Letters*, 89(16):162902, 2006.

[20] Anna N. Morozovska, Eugene A. Eliseev, and Maya D. Glinchuk. Size effects and depolarization field influence on the phase diagrams of cylindrical ferroelectric nanoparticles. *Physica B: Condensed Matter*, 387(1-2):358 – 366, 2007.

[21] J. Zhang, A. Heitmann, S. Alpay, and G. Rossetti. Electrothermal properties of perovskite ferroelectric films. *Journal of Materials Science*, 44:5263–5273, 2009. 10.1007/s10853-009-3559-8.

[22] Li-Ben Li, Jian Zhang, Zhen Yin, and Ming-Sheng Zhang. Position-thickness-dependent stresses and stress-induced diffuse dielectric anomaly in perovskite ferroelectric films. *Physics Letters A*, 321(1):67 – 73, 2004.

[23] A. M. Bratkovsky and A. P. Levanyuk. Smearing of phase transition due to a surface effect or a bulk inhomogeneity in ferroelectric nanostructures. *Phys. Rev. Lett.*, 94(10):107601, Mar 2005.

[24] E. C. Subbarao. Ferroelectric and antiferroelectric materials. *Ferroelectrics*, 5(1):267–280, 1973.

[25] Adrian Ciucivara, Bhagawan Sahu, and Leonard Kleinman. Density functional study of a ferromagnetic ferroelectric $lamno_3?batio_3$ superlattice. *Phys. Rev. B*, 77(9):092407, Mar 2008.

[26] F. Jona and G. Shirane. *Ferroelectric crystals*. Dover books on engineering. Dover Publications, 1993.

[27] Wenhui Ma and Dietrich Hesse. Microstructure and piezoelectric properties of sub-80 nm high polycrystalline srbi2ta2o9 nanostructures within well-ordered arrays. 85(15):3214–3216, 2004.

Appendix A

MATLAB and Igor Code

A.1 NEWALG114

- since the depolarization field is E = (2*lambda) / (epsilon*d) * P

```
function [W,AVALS] = NEWALG114(a, b, N, init,maxIter, TOL,lambda,...
    lambdaScreen,T,curved,stressed,Eterm0,busted,otherbusted)


tic;
if(nargin < 8)
    T = 300;
    lambdaScreen = .05e-9;
end
if(nargin <9)
    curved = 1;
    stressed = 1;
end
if (nargin < 12)
```

```
    Eterm0 = 0;
end
if (nargin <13)
    busted = 0;
end
if (nargin <14)
    otherbusted = 0;
end

%%%%%%%% PZT constants
% Tc = 666;
% SSNalpha0 = -4.887e7*2;
% SSNalphaT = SSNalpha0 / (300 - Tc);
%
% SSNalpha = SSNalphaT * (T - Tc);
%
% SSNbeta = 4.764e7*4;
% SSNgamma = 1.336e8*6;
% SSND = .45e-9;%% this is little g            sqrt(1e-19);
% mu = 5; %50;
% if busted
%     mu = 50;
% end
% Q12 = -4.6e-2;
% Q11 = 9.6e-2;
% %epsilon0 = 8.854e-12;
```

```
% chi33=2000;
%%%%%%%%%%%%%%%%%%%%

% % %%%%%%%% BTO constants - Li
% Tc = 393;
% SSNalpha0 = -4.887e7*2;
% % SSNalpha0 = -2.739e7*2;
% % SSNalphaT = SSNalpha0 / (300 - Tc);
% %
% % SSNalpha = SSNalphaT * (T - Tc);
% SSNalpha = 3.34*(T-381)*1e5;
% % SSNbeta = 5.4e8*4;
% % SSNgamma = .7e8*6;
% SSNbeta = (3.6*(T-448)*1e6)*4;
% SSNgamma = 4.9e8*6;
% SSND = .45e-9;%% this is little g            sqrt(1e-19);
% mu = 5; %50;
% % if busted
% %     mu = 50;
% % end
% Q12 = -4.5e-2;
% Q11 = 11e-2;
% epsilon0 = 8.854e-12;
% chi33=240;
% % %%%%%%%%%%%%%%%%%%%%
% %
```

```
% %%%%%%%% BTO constants - 2nd Try (Zhang JMaterSci)
Tc = 393;
% SSNalpha0 = -4.887e7*2;
% % SSNalpha0 = -2.739e7*2;
% SSNalphaT = SSNalpha0 / (300 - Tc);
% %
%SSNalpha = SSNalphaT * (T - Tc);
SSNalpha = 3.3*(T-383)*1e5*2;
% SSNbeta = 5.4e8*4;
% % SSNgamma = .7e8*6;
SSNbeta = (3.6*(T-448)*1e6)*4;
SSNgamma = 6.6e9*6;
SSND = .45e-9;%% this is little g            sqrt(1e-19);
mu = 5; %50;
if busted
    mu = 50;
end
Q12 = -4.3e-2;
Q11 = 11e-2; %from Li
epsilon0 = 8.854e-12;
chi33=240;
% %%%%%%%%%%%%%%%%%%%%%


% %%%%%%%% BTO constants - Hlinka
% %%%%% Way too high - approx 1.1
% % Tc = 393;
```

```
% % SSNalpha0 = -4.887e7*2;
% % SSNalpha0 = -2.739e7*2;
% % SSNalphaT = SSNalpha0 / (300 - Tc);
% %
% % SSNalpha = SSNalphaT * (T - Tc);
% SSNalpha = 2.772e7*2;
% SSNbeta = -6.476e8*4;
% % SSNgamma = .7e8*6;
% % SSNbeta = (3.6*(T-393)*1e6-202)*4;
% SSNgamma = 3.23e8*6;
% SSND = .45e-9;%% this is little g            sqrt(1e-19);
% mu = 5; %50;
% if busted
%     mu = 50;
% end
% Q12 = -4.3e-2;
% Q11 = 11e-2;
% %epsilon0 = 8.854e-12;
% chi33=240;
% %%%%%%%%%%%%%%%%%%%%

%%%%%%%%%% Depolarization thinger

since the depolarization field is E = (2*lambda) / (epsilon*d) * P

%%% we'll have depol = (2*lambda)/(epsilon*d)
```

```
%%% for now lambda is the same as our extrapolation length, but this could
%%% change - epsilon will be approximated as bulk (need a value for that)
epsilon0 = 8.85e-12; % free space
epsilon = epsilon0 * 800;

depol = (2*lambdaScreen)/(epsilon*abs(b-a));
%%%%%%%%%%

%%% initialize W
if length(init) == N
    W = init;
else
    W = zeros(N,1) + init;
end



%%% help calc Pbar - now calc it later
rvec = linspace(a,b,N);
sumrvec = sum(rvec);

%%% initialize constants
H = (b-a)/(N-1);
N1 = N-1;



%%%%%%%%%% Initialize our vectors for the Jacobian
```

```
A = zeros(N,1);
B = zeros(N,1);
C = zeros(N,1);
FF = zeros(N,1);
%%%%%%%%%%%%%%%%%%%%%% Speed things up? (yes, a lot)
SigRR = zeros(N,1);
SigA = zeros(N,1);
if stressed
    for x = 1:N
        SigRR(x) = CylStress(a + (x-1)*H,a,b,mu);
        SigA(x) = CylStressAz(a + (x-1)*H,a,b,mu);
    end
end

AVALS = zeros(N,1);
for x = 1:N
    AVALS(x) = SSNA(a + (x-1)*H,x);
end
%%%%%%%%%%%%%%%%%%%%%%%%%%%%%%%%%%%%

%%%%%%%%% here we go!
K = 1;
while (K <= maxIter)

    %%% update Pbar:
```

```
Pbar = dot(W,rvec)/sumrvec;
Eterm = Eterm0 + Pbar* 4*pi * 2;%/epsilon0 ;
if otherbusted == 1
    Eterm = Eterm0;
end


A(1) = 1 + lambda/H;
C(1) = -lambda/H;
FF(1) = -(W(1) - lambda * (W(2) - W(1))/H);
%X = a;

for I = 2:N1
    X = a  + (I - 1) * H;

    A(I) = 2 + H*H*FY(X, W(I), (W(I+1)-W(I-1))/(2*H),I);
    fyp = FYP(X,W(I),(W(I+1)-W(I-1))/(2*H),I);
    B(I) = -1 + .5 * H * fyp;
    C(I) = -1 - .5 * H * fyp;

    FF(I) = -(-(W(I-1) - 2*W(I) + W(I+1)) + H*H*F(X,W(I),(W(I+1)-W(I-1))/(2*H)

end


A(N) = 1 + lambda/H;
```

```
    B(N) = -lambda/H;
    FF(N) = -(W(N) + lambda * (W(N) - W(N-1))/H);

    J = sparse(1:N,1:N,A(1:N),N,N) + sparse(1:N-1,2:N,C(1:N-1),N,N) + sparse(2:N,1

    v = J\FF;


    W = W + v;

 %   fprintf('K=%d --- a: %g -- b: %g -- maxv: %e\n',K,W(1),W(N),max(abs(v)));
    if(max(abs(v)) < TOL || max(abs(W)) < 1e-7)
        fprintf('K=%d --- a: %g -- b: %g -- maxv: %e\n',K,W(1),W(N),max(abs(v)));
        fprintf('completed after %d (hurrah)!\n',K);
        if max(abs(v)) > TOL
            fprintf('Exited on "condition 2"');
        end
        toc;
        return;
    end



    K = K + 1;
end
```

```
fprintf('algorithm failed to converge');
toc;



    function F1 = F(r,p,pp,ind)
        F1 = 1/SSND * (AVALS(ind) * p + SSNbeta * p^3 + SSNgamma * p^5) - pp/r * c
    end

    function F2 = FY(r,p,pp,ind)
        F2 = 1/SSND*(AVALS(ind) + 3 * SSNbeta * p^2 + 5 * SSNgamma * p^4);
    end

    function F3 = FYP(r,p,pp,ind)
        F3 = -1/r * curved;
    end

    function Aval = SSNA(r,ind)
        %         [sigmac, dersig] = Sig2(r,AA,BB);
        %   Aval = SSNalpha - 2 * Q12 * C33 * sigmac * BETA;% * AA;
        %         Aval = (SSNalpha * 1) - 2 * Q12 * sigmac*AA *2e8;%* (1 + (BB-AA)


 %       pb = -mu / b;
%        pa = +mu / a;
        %            pave = (p1 + p2)/2;
%        if stressed
```

```
            sig = SigRR(ind);%CylStress(r,a,b,mu);
            siga = SigA(ind);
%         else
   %          sig= 0;%* stressed;% = (1 / (1 - (a/b)^2)) * ( pb*(1-(a/r)^2) + (a/b)
  %       end
         %             sig = (1 / (1 - (AA/BB)^2)) * (p1 + (AA/BB)^2 * p2);
         %             Aval = (SSNalpha * 1) - 2 * Q12 * pb ;
         Aval = SSNalpha - 2 * Q12 * siga - 2 * Q11 * sig;
         if(otherbusted)
             Aval = Aval + depol;
         else
             Aval = Aval -2 * 4 * pi;%/epsilon0;% depol;
         end

         if(busted) % for comparison with how things went wrong in the past
             Aval = SSNalpha - 2 * Q12 * sig + depol;
         end
         %   Aval = SSNalpha;
     end
end
```

A.2 CylStress

```
function s = CylStress(r,a,b,mu)
b = -b;
```

```
pb = +mu / b;

pa = -mu / a;

%            pave = (p1 + p2)/2;

% ab = a/b;

% ab2 = ab^2;

% ar = a/r;

% ar2 = ar^2;

% br = b/r;

% br2 = br^2;

%

% left = pb*(1-ar2);

% right = ab2*(1-br2)*pa;

% s = (1 / (1 - ab2)) * ( left + right);

s = (-1 / (1 - (a/b)^2)) * ( pb*(1-(a/r)^2) + (a/b)^2*(1-(b/r)^2)*pa);

end
```

A.3 CylStressAz

```
function s = CylStressAz(r,a,b,mu)

b = -b;

pb = +mu / b;

pa = -mu / a;

%            pave = (p1 + p2)/2;

% ab = a/b;

% ab2 = ab^2;
```

```
% ar = a/r;
% ar2 = ar^2;
% br = b/r;
% br2 = br^2;
%
% left = pb*(1-ar2);
% right = ab2*(1-br2)*pa;
% s = (1 / (1 - ab2)) * ( left + right);
s = (1 / (1 - (a/b)^2)) * ( pb*(1+(a/r)^2) + (a/b)^2*(1+(b/r)^2)*pa);
% if s < -43e9
%     s = -43e9;
%end
end
```

A.4 NALGwrapper

```
function [bigssn, mns] = NALGwrapper(a,b,pts,init,maxtry,tol,lambda1,lambda2,ts,..
    mnstol,curved,stressed)

mns = zeros(length(ts),1);
bigssn = zeros(pts,length(ts));
r = linspace(a,b,pts);
for x = 1:length(ts)
    if x==1
        bigssn(:,x)=NEWALG114(a,b,pts,init,maxtry,tol,lambda1,lambda2,ts(x),curved
```

```
        %bigssn(:,x)=NEWALG114(a,b,5000,1,100,1e-7,1e-9,.05e-9,ts(x));
    else
        bigssn(:,x)=NEWALG114(a,b,pts,bigssn(:,x-1),maxtry,tol,lambda1,lambda2,ts(
        %bigssn(:,x)=NEWALG114(a,b,5000,bigssn(:,x-1),100,1e-7,1e-9,.05e-9,ts(x));
    end

    if curved == 1
        mns(x)= dot(r,bigssn(1:pts,x))/sum(r);%mean(bigssn(1:5000,x));
    else
        mns(x) = mean(bigssn(1:pts,x));
    end

    fprintf('\n\n%d: %g %g\n%g\n\n',x,a,b,mns(x));
    if(abs(mns(x)) < mnstol)
        break;
    end
end
end
```

A.5 Poft

```
function [pmat,Eoft,tlist,mnslist] = Poft(p0, AVALS, beta, gamma,D, E0, dt, omega,
%[dpdt,left, right] = Poft(p0, AVALS, beta, gamma,D, E0, dt, omega,GAMMA, H)
tic;
```

```
N = length(p0);
N1 = N-1;

dpdt = zeros(N,1);
pmat = zeros(N,maxsteps);
tlist = ((1:maxsteps)-1)*dt;
Eoft = zeros(maxsteps,1);
mnslist = zeros(maxsteps,1);
% left = zeros(N,1);
% right = zeros(N,1);
%t = 0;
p = p0;

%%%%%%%%%%%%%%%%% Find ad-hoc coeffs k1, kN

k1 = abs( (AVALS(1)*p(1) + beta*p(1)^3 + gamma*p(1)^5)/((p(2)-p(1))/(H*H)*D));
kN = abs( (AVALS(N)*p(N) + beta*p(N)^3 + gamma*p(N)^5)/((p(N)-p(N1))/(H*H)*D));



for ts = 1:maxsteps
    t = tlist(ts);
    %%%%% Fill dpdt
    Eterm = - E0*sin(omega*t);
    Eoft(ts) = Eterm;
k1=1;
```

```
    s1 = 2*pi*p(1)*a/1e-9;
    dpdt(1) = AVALS(1)*p(1) + beta*p(1)^3 + gamma*p(1)^5 + (p(2)-p(1))/(H*H)*D * k

    % left(1) = AVALS(1)*p(1) + beta*p(1)^3 + gamma*p(1)^5;
    % right(1) = +(p(2)-p(1))/(H*H)*D;

    for n=2:N1
        %     left(n) = AVALS(n)*p(n) + beta*p(n)^3 + gamma*p(n)^5;
        %     right(n) = - (p(n+1)-2*p(n)+p(n-1))/(H*H)*D;
        dpdt(n) = AVALS(n)*p(n) + beta*p(n)^3 + gamma*p(n)^5 - (p(n+1)-2*p(n)+p(n-
    end
    dpdt(N) = AVALS(N)*p(N) + beta*p(N)^3 + gamma*p(N)^5 + (p(N)-p(N1))/(H*H)*D*kN
    % left(N) = AVALS(N)*p(N) + beta*p(N)^3 + gamma*p(N)^5;
    % right(N) = +(p(N)-p(N1))/(H*H)*D;
    %%%%%

    p = p + dpdt*dt/GAMMA;
    pmat(:,ts) = p;
    if(any(isnan(p)))
        fprintf('nans away! %d\n',ts);
        break;
    end
    mnslist(ts) = mean(p);
end
toc;
end
```

A.6 SolveForV

```
function W = SolveForV(P,R,lambda,init,maxIter,TOL)
tic;

if(length(P) ~= length(R))
    fprintf('Oh noes!');
    W = -1;
    return;
end



N = length(P);
W = ones(N,1) * init;
%W = linspace(1,-1,N)' * init;

N1 = N - 1;

%%%%%%%%%% Initialize our vectors for the Jacobian
A = zeros(N,1);
B = zeros(N,1);
C = zeros(N,1);
FF = zeros(N,1);

PP = zeros(N,1);
PPP = zeros(N,1);
```

```
%%%%%% Now some vectors for P and PP (they're const)
for I = 2:N1
    PP(I) = (P(I+1) - P(I-1))/(R(I+1) - R(I-1));
    PPP(I) = (P(I+1) - 2*P(I) + P(I-1))/((R(I+1) - R(I-1))/2)^2;
end

PP(1) = P(2) - (R(2)-R(1))*  (PP(3)-PP(2))/(R(3)-R(2));
PPP(1) = P(2) - (R(2)-R(1))*  (PPP(3)-PPP(2))/(R(3)-R(2));

PP(N) = P(N1) + (R(N)-R(N1))*  (PP(N1)-PP(N1-1))/(R(N1)-R(N1-1));
PPP(N) = P(N) + (R(N)-R(N1))*  (PPP(N1)-PPP(N1-1))/(R(N1)-R(N1-1));
%%%%%%%%%%%%%%%%%%%%%%%%%%%%%%%%%%%%%%%%%%%%%%%%%%%%%%%%

%%%%%%%%%% here we go!
K = 1;
while (K <= maxIter)

    H = R(2) - R(1);
%     A(1) = -1;%/H;
%     C(1) = 1;%/H;
%     FF(1) = -(W(2) - W(1));%/H;
%
%      A(1) = 1 + lambda/H; %% good version
%      C(1) = -lambda/H;
%      FF(1) = -(W(1) - lambda * (W(2) - W(1))/H);
%
```

```
% Prev version
   A(1) = 1 - R(1)/H; %% Grad V = 0 %% this is the version we liked
   C(1) = +R(1)/H;
   FF(1) = -(W(1) + R(1) * (W(2) - W(1))/H);

%     A(1) = -1000000;% 1 + lambda/H * 0;
%     C(1) = 0;%-lambda/H * 0;
%     FF(1) = -(W(2) - W(1));% -(W(1) - lambda * (W(2) - W(1))/H * 0);

%
%     A(1) = 1 - lambda/H; %% Trying opp sign for lambda
%     C(1) = +lambda/H;
%     FF(1) = -(W(1) + lambda * (W(2) - W(1))/H);

    for I = 2:N1
        H = (R(I+1)-R(I-1))/2;

        X = R(I);%a  + (I - 1) * H;

        A(I) = 2 ;%+ H*H*FY(X, W(I), (W(I+1)-W(I-1))/(2*H),I);
        fyp = Fvp(X);%FYP(X,W(I),(W(I+1)-W(I-1))/(2*H),I);
        B(I) = -1 + .5 * H * fyp;
        C(I) = -1 - .5 * H * fyp;

        FF(I) = -(-(W(I-1) - 2*W(I) + W(I+1))...
```

```
            + H*H*Vrr(X,(W(I+1)-W(I-1))/(2*H),P(I),PP(I)));

    end

    H = R(N) - R(N1);
%     A(N) = 1;%/H;
%     B(N) = -1;%/H;
%     FF(N) = -(W(N) - W(N-1));%/H;

%     A(N) = 1 + lambda/H; %% sort of working
%     B(N) = -lambda/H;
%     FF(N) = -(W(N) + lambda * (W(N) - W(N-1))/H);

%prev
    A(N) = 1 + R(N)/H; %% this is the version we liked
    B(N) = -R(N)/H;
    FF(N) = -(W(N) + R(N) * (W(N) - W(N-1))/H);

    J = sparse(1:N,1:N,A(1:N),N,N) + sparse(1:N-1,2:N,C(1:N-1),N,N) + sparse(2:N,1

    v = J\FF;


    W = W + v;

    fprintf('K=%d --- a: %g -- b: %g -- maxv: %e\n',K,W(1),W(N),max(abs(v)));
```

```
    if(max(abs(v)) < TOL% || max(abs(W)) < 1e-7)
        fprintf('completed after %d (hurrah)!\n',K);
        if max(abs(v)) > TOL
            fprintf('Exited on "condition 2"');
        end
        toc;
        return;
    end




    K = K + 1;
end

fprintf('algorithm failed to converge');
toc;

%%%%%%%%%%%%%% INLINE FUNCTIONS %%%%%%%%%%%%%
    function vrr = Vrr(r, Vp, p, Pp)
        vrr = -(p/r + Pp + Vp/r);
    end

    function fr = Fr(r, Vp, p, Pp, Ppp)
        fr = -(-p/r^2 + Ppp - Vp/r + -(p/r + Pp + Vp/r));
    end
```

```
    function fv = Fv()
        fv = 0;
    end

    function fvp = Fvp(r)
        fvp = -1/r;
    end
end
```

A.7 ThermalPofE

```
function [ps,ms,mnsp,mnsm,rv] = ThermalPofE(a,b,N,ef,T,curved)

if(nargin < 6)
    curved = 1;
end
% T = 300;
% N = 1000;
% a = 90e-9;
% b = 120e-9;

ps = zeros(1000,N);
ms = zeros(1000,N);
mnsp = zeros(N,1);
mnsm = zeros(N,1);
```

```
rv = linspace(a,b,1000);



%ef = 1e14;
t1 = rem(now,1);

eees = zeros(N,1);
for x = 1:N
    eees(x) = -(x-1)*ef;%/10000-6.155e16;
end









last = -ones(1000,1);

for x = 1:N
   ms(:,x) = NEWALG114(a,b, 1000,last,500,1e-9,1e-9,.05e-9,T,curved,curved,eees(x)

   last = ms(:,x);
   fprintf('\n\n\n%d done (minus)\n\n\n',x);
end

last = ones(1000,1);
```

```
for x = 1:N

   ps(:,x) = NEWALG114(a,b,1000,last,500,1e-9,1e-9,.05e-9,T,curved,curved,eees(x))

   last = ps(:,x);

   fprintf('\n\n\n%d done (plus)\n\n\n',x);
end



t2 = rem(now,1);

sm = sum(rv);
for x = 1:N
    mnsp(x) = dot(ps(:,x),rv)/sm;
    mnsm(x) = dot(ms(:,x),rv)/sm;
end




fprintf('took: %f min\n\n',(t2-t1)*24*60);




%
%
```

```
% eeesbig90a = eees;
% msbig90a = ms;
% psbig90a = ps;
% r90a = rv;
% mnsp90a = mnsp;
% mnsm90a = mnsm;
end
```

A.8 ssnSCRIPT

```
t1 = rem(now,1);

ts=linspace(0,600,500);

tscrvflat = ts;
mns = zeros(length(ts),1);
bigssn = zeros(5000,length(ts));

pts = 5000;
init = 1;
maxtry = 200;
tol = 1e-7;
lambda1 = 1e-9;
lambda2 = .05e-9;
mnstol = 1e-5;
```

```
%% curved
a = 18e-9;
b = 25e-9;
curved = 1;
stressed = 1;

[bigssn1825crv2,mns1825crv2] = NALGwrapper(a,b,pts,init,maxtry,tol,...
    lambda1,lambda2,ts,...
    mnstol,curved,stressed);

%
a = 29e-9;
b = 40e-9;
curved = 1;
stressed = 1;

[bigssn2940crv,mns2940crv] = NALGwrapper(a,b,pts,init,maxtry,tol,...
    lambda1,lambda2,ts,...
    mnstol,curved,stressed);



a = 40e-9;
b = 55e-9;
curved = 1;
stressed = 1;
```

```
[bigssn4055crv,mns4055crv] = NALGwrapper(a,b,pts,init,maxtry,tol,...
    lambda1,lambda2,ts,...
    mnstol,curved,stressed);



a = 90e-9;
b = 120e-9;
curved = 1;
stressed = 1;

[bigssn90120crv,mns90120crv] = NALGwrapper(a,b,pts,init,maxtry,tol,...
    lambda1,lambda2,ts,...
    mnstol,curved,stressed);

%% flat
a = 18e-9;
b = 25e-9;
curved = 0;
stressed = 0;

[bigssn1825flat,mns1825flat] = NALGwrapper(a,b,pts,init,maxtry,tol,...
    lambda1,lambda2,ts,...
    mnstol,curved,stressed);



a = 29e-9;
```

```
b = 40e-9;
curved = 0;
stressed = 0;

[bigssn2940flat,mns2940flat] = NALGwrapper(a,b,pts,init,maxtry,tol,...
    lambda1,lambda2,ts,...
    mnstol,curved,stressed);



a = 40e-9;
b = 55e-9;
curved = 0;
stressed = 0;

[bigssn4055flat,mns4055flat] = NALGwrapper(a,b,pts,init,maxtry,tol,...
    lambda1,lambda2,ts,...
    mnstol,curved,stressed);



a = 90e-9;
b = 120e-9;
curved = 0;
stressed = 0;

[bigssn90120flat,mns90120flat] = NALGwrapper(a,b,pts,init,maxtry,tol,...
    lambda1,lambda2,ts,...
```

```
    mnstol,curved,stressed);


a = 150e-9;

b = 200e-9;

curved = 0;

stressed = 0;


[bigssn150200flat,mns150200flat] = NALGwrapper(a,b,pts,init,maxtry,tol,...
    lambda1,lambda2,ts,...
    mnstol,curved,stressed);


t2 = rem(now,1);


fprintf('took %f minutes', (t2-t1)*24*60);
```

A.9 plots

```
T = 300;

p18 = NEWALG114(18e-9,25e-9,5000,11,200,1e-9,1e-9,.05e-9,T,1,1,0,0);

p29 = NEWALG114(29e-9,40e-9, 5000,11,200,1e-9,1e-9,.05e-9,T,1,1);

p40 = NEWALG114(40e-9,55e-9, 5000,11,200,1e-9,1e-9,.05e-9,T,1,1);

p90 = NEWALG114(90e-9,120e-9,5000,11,200,1e-9,1e-9,.05e-9,T,1,1);

p150 = NEWALG114(150e-9,200e-9,5000,11,200,1e-9,1e-9,.05e-9,T,1,1);


%
```

```
p18tf = NEWALG114(18e-9,25e-9,5000,1,200, 1e-9,1e-9,.05e-9,T,0,0,0,0);
p29tf = NEWALG114(29e-9,40e-9,5000,1,200, 1e-9,1e-9,.05e-9,T,0,0,0,0);
p40tf = NEWALG114(40e-9,55e-9,5000,1,200, 1e-9,1e-9,.05e-9,T,0,0,0,0);
p90tf = NEWALG114(90e-9,120e-9,5000,1,200,1e-9,1e-9,.05e-9,T,0,0,0,0);
p150tf = NEWALG114(150e-9,200e-9,5000,1,200,1e-9,1e-9,.05e-9,T,0,0,0,0);

% %  p18ob = NEWALG114(18e-9,25e-9,5000,1,200, 1e-9,1e-9,.05e-9,T,1,1,0,1);
% %  p29ob = NEWALG114(29e-9,40e-9,5000,1,200, 1e-9,1e-9,.05e-9,T,1,1,0,1);
% %  p40ob = NEWALG114(40e-9,55e-9,5000,1,200, 1e-9,1e-9,.05e-9,T,1,1,0,1);
% %  p90ob = NEWALG114(90e-9,120e-9,5000,1,200,1e-9,1e-9,.05e-9,T,1,1,0,1);
%
r18=linspace(18,25,5000)*1e-9;
r29=linspace(29,40,5000)*1e-9;
r40=linspace(40,55,5000)*1e-9;
r90=linspace(90,120,5000)*1e-9;
r150=linspace(150e-9,200e-9,5000);
% %
% %%  v18 = SolveForV(p18ob,r18,.5e-8,1e2,5000,1e-12);
%
% v18 = SolveForV(p18,r18,1e-9,1e4,5000,1e-12);
% v29 = SolveForV(p29,r29,1e-9,1e2,5000,1e-12);
% v40 = SolveForV(p40,r40,1e-9,1e2,5000,1e-12);
% v90 = SolveForV(p90,r90,1e-9,1e2,5000,1e-12);

% v18ob = SolveForV(p18ob,r18,1e-9,-1e2,5000,1e-12);
% v29ob = SolveForV(p29ob,r29,1e-9,-1e2,5000,1e-12);
```

```
% v40ob = SolveForV(p40ob,r40,1e-9,-1e2,5000,1e-12);
% v90ob = SolveForV(p90ob,r90,1e-9,-1e2,5000,1e-12);
%
% %
r18b = r18 - r18(1);
r29b = r29 - r29(1);
r40b = r40 - r40(1);
r90b = r90 - r90(1);
r150b= r150 - r150(1);
% %
figure; hold;
plot(r18b,p18,r29b,p29,r40b,p40,r90b,p90,r18b,p18tf,r29b,p29tf,r40b,p40tf,r90b,p90
% figure; hold;
% plot(r150b,p150tf,pbulkx,pbulk);
%figure; hold;
%plot(tscrvflat,mns1825crv2,tscrvflat,mns2940crv,tscrvflat,mns4055crv,tscrvflat,mn
%
% v18eo = v18ob/epsilon0;
% v29eo = v29ob/epsilon0;
% v40eo = v40ob/epsilon0;
% v90eo = v90ob/epsilon0;
%
% v18eb = v18e - v18e(1);
% v29eb = v29e - v29e(1);
% v40eb = v40e - v40e(1);
% v90eb = v90e - v90e(1);
```

```
%
%
% v18eob = v18eo - v18eo(1);
% v29eob = v29eo - v29eo(1);
% v40eob = v40eo - v40eo(1);
% v90eob = v90eo - v90eo(1);
%
%figure; hold;
% %plot(r18b,v18eob,'--',r29b,v29eob,'--',r40b,v40eob,'--',r90b,v90eob,'--');
% plot(r18b,v18eb ,r29b,v29eb ,r40b,v40eb ,r90b,v90eb );
% figure; hold;
% plot(r18b,v18eob,r29b,v29eob,r40b,v40eob,r90b,v90eob);
% %

% [ps18b,ms18b,mnsp18b,mnsm18b,rv18b] = ThermalPofE(18e-9,25e-9,1200,1e14,300);
% [ps29b,ms29b,mnsp29b,mnsm29b,rv29b] = ThermalPofE(29e-9,40e-9,1200,1e14,300);
% [ps40b,ms40b,mnsp40b,mnsm40b,rv40b] = ThermalPofE(40e-9,55e-9,1200,1e14,300);
% [ps90b,ms90b,mnsp90b,mnsm90b,rv90b] = ThermalPofE(90e-9,120e-9,1200,1e14,300);

% [psbigb,msbigb,mnspbigb,mnsmbigb,rvbigb] = ThermalPofE(1e-0,2e-0,1200,1e14,300);


%[psbigb,msbigb,mnspbigb2,mnsmbigb2,rvbigb] = ThermalPofE(100,102,5000,1e14,300,0)

% % % [psbiga,msbiga,mnspbiga,mnsmbiga,rvbiga] =
% % % ThermalPofE(119,120,1000,1e14,300);
```

```
% %
% %

%simplethermal(a, b, N, init,maxIter, TOL,lambda,...
%   lambdaScreen,Tmin, Tmax, steps,curved,stressed,Eterm,busted)
% [t18, mns18, big18] = simplethermal(18e-9,25e-9, 1000,1,500,1e-9,1e-9,...
%     .05e-9,0, 1500, 1500,1,1,0,0);
% [t29, mns29, big29] = simplethermal(29e-9,40e-9, 1000,1,500,1e-9,1e-9,...
%     .05e-9,0, 1500, 1500,1,1,0,0);
% [t40, mns40, big40] = simplethermal(40e-9,55e-9, 1000,1,500,1e-9,1e-9,...
%     .05e-9,0, 1500, 1500,1,1,0,0);
% [t90, mns90, big90] = simplethermal(90e-9,120e-9, 1000,1,500,1e-9,1e-9,...
%     .05e-9,0, 1500, 1500,1,1,0,0);

%
% [t18tf, mns18tf, big18tf] = simplethermal(18e-9,25e-9, 1000,1,500,1e-9,1e-9,...
%     .05e-9,0, 1500, 1500,0,0,0,0);
% [t29tf, mns29tf, big29tf] = simplethermal(29e-9,40e-9, 1000,1,500,1e-9,1e-9,...
%     .05e-9,0, 1500, 1500,0,0,0,0);
% [t40tf, mns40tf, big40tf] = simplethermal(40e-9,55e-9, 1000,1,500,1e-9,1e-9,...
%     .05e-9,0, 1500, 1500,0,0,0,0);
% [t90tf, mns90tf, big90tf] = simplethermal(90e-9,120e-9, 1000,1,500,1e-9,1e-9,...
%     .05e-9,0, 1500, 1500,0,0,0,0);

% plot(t18,mns18,t29,mns29,t40,mns40,t90,mns90)
%
```

```
%
%
% % %plots
% %
% % figure;
% % plot(r18_5-18e-9,p18,r29_5-29e-9,p29,r40_5-40e-9,p40,r90_5-90e-9,p90)
% %
% % figure;
% % plot(tsng2,abs(mns1825ng2),tsng2,abs(mns2940ng2),tsng2,abs(mns4055ng2),tsng2,a
% %
%
% % T = 300;
% % r18 = 1e-9 * linspace(18,25,5000);
% % r29 = 1e-9 * linspace(29,40,5000);
% % r40 = 1e-9 * linspace(40,55,5000);
% % r90 = 1e-9 * linspace(90,120,5000);
% %
% %  p18 = NEWALG114(18e-9,25e-9, 5000,1,200,1e-9,1e-9,.05e-9,T,1,1);
% % p29 = NEWALG114(29e-9,40e-9, 5000,1,200,1e-9,1e-9,.05e-9,T,1,1);
% % p40 = NEWALG114(40e-9,55e-9, 5000,1,200,1e-9,1e-9,.05e-9,T,1,1);
% % p90 = NEWALG114(90e-9,120e-9,5000,1,200,1e-9,1e-9,.05e-9,T,1,1);
% %
% % p18b = NEWALG114(18e-9,25e-9, 5000,1,200,1e-9,1e-9,.05e-9,T,1,1,0,1);
% % p29b = NEWALG114(29e-9,40e-9, 5000,1,200,1e-9,1e-9,.05e-9,T,1,1,0,1);
% % p40b = NEWALG114(40e-9,55e-9, 5000,1,200,1e-9,1e-9,.05e-9,T,1,1,0,1);
% % p90b = NEWALG114(90e-9,120e-9,5000,1,200,1e-9,1e-9,.05e-9,T,1,1,0,1);
```

```
% %
% % p18tf = NEWALG114(18e-9,25e-9, 5000,1,200,1e-9,1e-9,.05e-9,T,0,0);
% % p29tf = NEWALG114(29e-9,40e-9, 5000,1,200,1e-9,1e-9,.05e-9,T,0,0);
% % p40tf = NEWALG114(40e-9,55e-9, 5000,1,200,1e-9,1e-9,.05e-9,T,0,0);
% % p90tf = NEWALG114(90e-9,120e-9,5000,1,200,1e-9,1e-9,.05e-9,T,0,0);
%
% %
% %
%
% % v18big = zeros(5000, length(tscrvflat)/10);
% %
% % for x=1:length(tscrvflat)/10
% %     v18big(:,x)=SolveForV(bigssn1825crv(1:5000,x*10),r18,0,1e-5,1000,1e-12);
% % end
% %
% % v29big = zeros(5000, length(tscrvflat)/10);
% %
% % for x=1:length(tscrvflat)/10
% %     v29big(:,x)=SolveForV(bigssn2940crv(1:5000,x*10),r18,0,1e-5,1000,1e-12);
% % end
% %
% % v40big = zeros(5000, length(tscrvflat)/10);
% %
% % for x=1:length(tscrvflat)/10
% %     v40big(:,x)=SolveForV(bigssn4055crv(1:5000,x*10),r18,0,1e-5,1000,1e-12);
% % end
```

```
% %
% % v90big = zeros(5000, length(tscrvflat)/10);
% %
% % for x=1:length(tscrvflat)/10
% %     v90big(:,x)=SolveForV(bigssn90120crv(1:5000,x*10),r18,0,1e-5,1000,1e-12);
% % end
%
% % T=712;
% % Tc = 714;
% % dt = T - Tc;
% %
% % at0 = -4.887e7*2/-366;
% % beta = 4.764e7*4;
% % gamma = 1.336e8*6;
% % alpha = dt*at0;
% %
% % N = 3001;
% % rts = zeros(5,N);
% % Eps = zeros(N,1);
% %
% % for x = 1:N
% %     E = (x-(N-1)/2)*5e1;
% %     dp = (2*.05/(7*8.854e-12));
% %     Ep = E;
% %     rt = roots([gamma 0 beta 0 (alpha) -Ep]);
% %     rts(:,x) = rt;
```

```
% %     Eps(x) = Ep;
% % end
% %
% % maxr = zeros(N,1);
% % minr = zeros(N,1);
% % for x = 1:N
% %     maxr(x) = -inf;
% %     minr(x) = +inf;
% %     for y = 1:5
% %         if(isreal(rts(y,x)))
% %             if(rts(y,x) > maxr(x))
% %                 maxr(x) = rts(y,x);
% %             end
% %             if(rts(y,x) < minr(x))
% %                 minr(x) = rts(y,x);
% %             end
% %         end
% %     end
% % end
% %
%
% %
% % ind = 0;
% % exes = linspace(-1,1,5001)*.5;
% % vals = zeros(length(exes),1);
% % for x=exes
```

```
% %    ind = ind + 1;
% %    pp = x;
% %    pv = [pp^5 pp^4 pp^3 pp^2 pp^1 pp^0];
% %    cv = [gamma 0 beta 0 alpha -E*0];
% %    vals(ind) =dot(cv,pv);
% %
% % end
% %
% %
% % T = 300;
% % N = 1000;
% % a = 90e-9;
% % b = 120e-9;
% %
% % ps = zeros(1000,N);
% % ms = zeros(1000,N);
% % mnsp = zeros(N,1);
% % mnsm = zeros(N,1);
% %
% % rv = linspace(a,b,1000);
% %
% %
% % ef = 1e14;
% % t1 = rem(now,1);
% %
% % eees = zeros(N,1);
```

```
% % for x = 1:N
% %     eees(x) = -(x-1)*ef;%/10000-6.155e16;
% % end
% %
% %
% % last = ones(1000,1);
% % for x = 1:N
% %
% %    ps(:,x) = NEWALG114(a,b,1000,last,500,1e-9,1e-9,.05e-9,T,1,1,eees(x));
% %
% %    last = ps(:,x);
% %
% %    fprintf('\n\n\n%d done (plus)\n\n\n',x);
% % end
% %
% %
% % last = -ones(1000,1);
% %
% % for x = 1:N
% %    ms(:,x) = NEWALG114(a,b, 1000,last,500,1e-9,1e-9,.05e-9,T,1,1,eees(x));
% %
% %    last = ms(:,x);
% %    fprintf('\n\n\n%d done (minus)\n\n\n',x);
% % end
% % t2 = rem(now,1);
% %
```

```
% % sm = sum(rv);
% % for x = 1:N
% %     mnsp(x) = dot(ps(:,x),rv)/sm;
% %     mnsm(x) = dot(ms(:,x),rv)/sm;
% % end
% %
% %
% %
% % fprintf('took: %f min\n\n',(t2-t1)*24*60);
% %
% %
% %
% %
% %
% % eeesbig90a = eees;
% % msbig90a = ms;
% % psbig90a = ps;
% % r90a = rv;
% % mnsp90a = mnsp;
% % mnsm90a = mnsm;
```

A.10 Coercive Voltage Igor Procedure

```
Function H2RGB(h)
variable h
```

```
variable s, v, hi, f, p, q, t
variable r = 0, g = 0, b = 0

s = 1
v = 1

hi = mod(floor(h/60), 6)

f  = h/60 - hi
p = v * (1 - s)
q= v * (1 - f * s)
t = v * (1 - (1 -f) * s)

if(hi == 0)
r = v
g = t
b = p
endif
if(hi == 1)
r = q
g = v
b = p
endif
if(hi == 2)
r = p
```

```
g = v
b = t
endif
if(hi == 3)
r = p
g = q
b = v
endif
if(hi == 4)
r = t
g = p
b = v
endif
if(hi == 5)
r = v
g = p
b = q
endif

make/o/n=3 RGB

RGB[0] = r
RGB[1] = g
RGB[2] = b

rgb *= 65535
```

```
return RGB
end // hsv2rgb

function h2r(h)
variable h
wave rgb

rgb = h2rgb(h)

return rgb[0]
end //h2r

function h2g(h)
variable h
wave rgb

rgb = h2rgb(h)

return rgb[1]
end //h2g

function h2b(h)
variable h
wave rgb
```

```
rgb = h2rgb(h)

return rgb[2]
end //h2b

macro cleverIntegral(ywave, xwave,maxX) //, [x1, x2, x3, x4])
string ywave, xwave
variable maxX
// variable x1, x2, x3, x4

// wave ywave = $ywavestr
// wave xwave = $xwavestr

if(maxX < 0)
maxX = inf
endif

variable origlength = dimsize($xwave, 0)



variable mincount = findmins($xwave)

//wave mw = mw

make/o/n=(origlength - 1) avg2p, areas, dxwave, dywave, yareas, avg2px
```

```
avg2p = 0
areas = 0
dxwave = 0
yareas = 0
avg2px = 0

dxwave[0,]  = ($xwave[p+1] - $xwave[p]) * -1
dywave[0,]  = ($ywave[p+1] - $ywave[p]) * -1
avg2p[0,] = ($ywave[p+1] + $ywave[p])/2
avg2px[]  = ($xwave[p] + $xwave[p + 1]) / 2

areas[] = dxwave[p] * avg2p[p] * ($xwave[p] < abs(maxX))
// yareas[] = (-2 * ((dxwave[p] > 0) - .5)) * dywave[p] * avg2px[p]
yareas[] = dywave[p] * avg2px[p] * -1* ($xwave[p] < abs(maxX))


if(1) // if(paramisdefault(x1))
variable i, ts, s, ys, yts
string ysumstr = ywave + "_sum"
string ysumstr2 = ywave + "_sum2"
string ysub, xsub
make/o/n=(mincount - 1) $ysumstr $ysumstr2

//wave ysum = $ysumstr

display /k=1
```

```
//for(i = 0, ts = 0, s = 0; i < mincount-1; i = i +1)
i = 0
s = 0
ts = 0
ys = 0
yts = 0
make /o/n=3 rgb
if(i < mincount -1)
do
s = simplesum2(areas, mw[i], mw[i + 1])
$ysumstr[i] = s
ts = ts + s

ys = simplesum2(yareas, mw[i], mw[i+1])
$ysumstr2[i] = ys
yts += ys

ysub = (ywave + "_sub" + num2str(i))
xsub = (ywave + "_xsub" + num2str(i))
make/o/n=(mw[i+1] - mw[i] + 1) $ysub, $xsub

$ysub[] = $ywave[p + mw[i]]
$xsub[] = $xwave[p + mw[i]]

h2rgb(i * (280 / mincount))
```

```
appendtograph $ysub vs $xsub
modifygraph rgb($ysub)=(rgb[0],rgb[1],rgb[2])

i = i + 1
while(i < mincount - 1)
display /k=1 $ysumstr
print mw
endif
//endfor



// wavestats/q areas
// print  areas[v_maxloc] * dxwave[v_maxloc]



variable weightedx = weightedavg($xwave, areas, mw[0], mw[mincount-1])
print "avg x:", weightedx


print "total area", ts / (mincount - 1)
//return


variable weightedy = weightedavg($ywave, yareas, mw[0], mw[mincount-1])
print "avg y:", weightedy
```

```
print "other area calc:", simplesum2(areas, mw[0], mw[mincount-1]) / (mincount - 1

print "otherother area calc:", yts / (mincount - 1)

variable vc = FindVC($xwave, $ywave, weightedy, mw[0], mw[mincount-1], 0)
print "VC:", vc

// FindVC($xwave, $ywave, 0, mw[0], mw[mincount-1], 0)

print
variable vd = FindVC($ywave, $xwave, weightedx, mw[0], mw[mincount-1], 1)
print "VD:", vd

return
endif

variable s1, s2

s1 = simplesum2(areas, x1, x2)
s2 = simplesum2(areas, x3, x4)

print s1, s2

return s1 + s2
end //cleverintegral
```

```
function simplesum(w)
wave w

variable length = dimsize(w, 0)

variable i, s

for(i = 0, s = 0; i < length; i = i + 1)
s = s + w[i]
endfor

return s
end // simplesum

function simplesum2(w, x1, x2)
wave w
variable x1, x2

variable step  = ((x2 > x1) - .5) * 2

variable length = dimsize(w, 0)

variable i, s

for(i = x1, s = 0; i < length && i > 0 && i < max(x1, x2) && i >= min(x1, x2); i =
```

```
s = s + w[i]
endfor

return s
end  // simplesum2

function findmins(w1)
wave w1

variable length = dimsize(w1, 0)

make/o/n=0 mw

variable i, count

for(i = 1, count = 0; i < length - 1; i = i  + 1)
if(w1[i] < w1[i - 1]  && w1[i] < w1[i + 1] && (count == 0 || i > 99 + mw[count - 1
redimension /n=(count + 1) mw
mw[count] = i
count = count + 1
endif
endfor

duplicate/o mw mwy

mwy[] = w1[mw[p]]
```

```
display /k=1 w1
appendtograph mwy vs mw
ModifyGraph mode(mwy)=3,marker(mwy)=29

print "count ",count
return count
end // findmins

function weightedavg(weightwave, valuewave, start, stop)
wave weightwave, valuewave
variable start, stop

variable weighted, totalvalue, i

for(i = start, weighted = 0, totalvalue = 0; i < stop; i += 1)
weighted += weightwave[i] * valuewave[i]
totalvalue += valuewave[i]
endfor

return weighted / totalvalue
end //weightedavg


function findVC(xwave, ywave, yavg, start, stop, reversed)
wave xwave, ywave
```

```
variable yavg, start, stop,reversed

make/n=0/o set1, set2, xset, yset
variable i


for(i = start; i < stop; i += 1)
if((ywave[i] > yavg && ywave[i + 1] <= yavg) || (ywave[i] < yavg && ywave[i + 1] >
if( (!reversed && xwave[i] > xwave[i + 1])  || (reversed && ywave[i] > ywave[i + 1
InsertPoints 0, 1, set1
set1[0] = findlinearzero(xwave[i], ywave[i] - yavg, xwave[i + 1], ywave[i + 1] - y
insertpoints 0, 1, xset
xset[0] = xwave[i]
insertpoints 0, 1, yset
yset[0] = ywave[i]
else
InsertPoints 0, 1, set2
set2[0] = findlinearzero(xwave[i], ywave[i] - yavg, xwave[i + 1], ywave[i + 1] - y
insertpoints 0, 1, xset
xset[0] = xwave[i]
insertpoints 0, 1, yset
yset[0] = ywave[i]
endif
endif
endfor
```

```
print "s1", mean(set1)
print "s2", mean(set2)

print "diff:", abs(mean(set1) - mean(set2))

return abs(mean(set1) - mean(set2))
end //FindVC



function findLinearZero(x1, y1, x2, y2)
variable x1, y1, x2, y2

variable m

m = (y2 - y1) / (x2 - x1)

return x1 - y1 / m

end //findLinearZero

macro testmacro(t)
variable t

if(t < 0)
t = inf
endif
```

```
print t > 1000


end
```

Appendix B

BTO Material Constants

Landau Coefficient	
A	3.3*(T-383)*1e5
B	3.6*(T-448)*1e6
C	6.6e9
Electrostrictive Coefficients	
Q_{12}	-4.3e-2
Q_{11}	11e-2

Table B.1: BTO Constant Values [21, 22]